# Biodegradable magnesium implants, immunomodulation, and tissue repair/regeneration

**Heithem Ben Amara**

Department of Biomaterials
Institute of Clinical Sciences
Sahlgrenska Academy, University of Gothenburg

UNIVERSITY OF GOTHENBURG

*Gothenburg 2023*

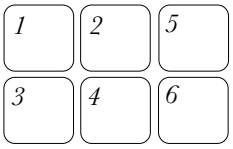


*Cover illustration: The response of tissues of different natures at the interface with biodegradable metallic magnesium implants under examination with different microscopic modalities. The micrographs show histological sections of bone (1) in contact with a magnesium implant, and inflammatory cells recruited to soft tissue (2, 3) interfacing with a magnesium implant. The arrangement of cells around gas bubbles deriving from the implant degradation in tissues was revealed by scanning electron microscopy (4), immunohistochemistry (5), and investigated with image analysis (6).*

Biodegradable magnesium implants, immunomodulation, and tissue repair/regeneration


heithem.ben.amara@biomaterials.gu.se

ISBN 978-91-8069-483-4 (PRINT)
ISBN 978-91-8069-484-1 (PDF)
http://hdl.handle.net/2077/77760

Printed by Stema Specialtryck AB, Borås, Sweden 2023

*Learning without thought is labor lost;*
*thought without learning is perilous.*

Confucius

# *Abstract*

The century-old paradigm of holding fractures with a metallic implant to enable bone repair, known as osteosynthesis, is still used today without alteration. Patients are increasingly being treated with metallic implants made of magnesium (Mg) that secure osteosynthesis and are reabsorbed *in situ* without the surgical re-entry that requires their permanent analogs. Often, Mg implants achieve osteosynthesis. However, when failure occurs, aberrant inflammation in overlaying soft tissue and persistent peri-implant radiolucencies generated by gas release from the implants are common. How can this be reconciled with popular concepts predestining Mg implants to promote bone formation by mitigating inflammation and bone resorption? This thesis investigated the sequence of biological processes prompting soft tissue and bone to accommodate Mg implants with different degradation behaviors from early to relatively long healing. Detailed studies of cells and their molecular circuits during inflammation were undertaken in different but related biological compartments surrounding the implants. Complementary analytical microscopy and compositional spectroscopy were performed to characterize tissue assembly at the interface with the implants and beyond. Compared to nondegradable titanium implants, Mg implants amplify initial inflammation in soft tissue and bone. The rapid release of degradation products, including $Mg^{2+}$ and gas, correlatively induces a strong, transient proinflammatory environment that fosters mRNA and protein programs associated with macrophage polarization, chemotaxis, osteoclastogenesis, and neovascularization but without cytotoxic effects. Thereafter, inflammation markedly subsides. The transition to soft tissue and bone repair coincides with the attenuation of $Mg^{2+}$ concentrations and gas void generation in the peri-implant milieu in tandem with an enrichment in calcium and phosphorous on the implant surface. Immunomodulation by Mg implants, reflected by a shift from proinflammatory to prohealing macrophage activation, reinforces their anchorage in bone and alleviates fibrotic encapsulation in soft tissue. However, this restorative effect is not equal in response to the various Mg degradation behaviors. Pure Mg implants, which degrade faster than clinical-grade alloyed Mg implants, alter the composition of interfacial bone and result in a previously unknown proadipogenic response in the bone marrow beyond the bone–implant interface. This increased adiposity is closely associated with persistent gas voids in bone marrow. Gas voids encourage inflammation in their microenvironment, trigger mechanosensation, and may induce local bone matrix deposition. In conclusion, Mg implants in different tissues transiently amplify the initial immune reaction, and degradation product escape creates an inflammatory microenvironment at the tissue–implant interface and beyond. An appropriate reparative response is obtained but can be impaired by the uncontrolled implant degradation. Above the demand for rigorous tailoring of Mg implants, healing monitoring needs to expand to tissues outside the confines of the implant interface, with pending questions on the fate of tissues under compromised conditions.



**Keywords:** *Adipose tissue; Biodegradable implants; Bone–implant interface; Bone marrow; Inflammation; Cellular mechanotransduction; Gene expression; Immunohistochemistry; Magnesium; Neovascularization; Osseointegration; Soft tissue injuries*

# *Sammanfattning på svenska*

Läkning av benbrott med hjälp av kirurgiskt fixerade benändar och icke-nedbrytbara implantat (osteosyntes) är en rådande behandlingsprincip. Under senare år har ett ökat antal patienter behandlats med nedbrytbara magnesium (Mg) implantat som dels förankrar benändarna, dels bryts ner i kroppen. Under förutsätttningen att vävnaden läks så har denna behandling fördelen att en eventuell kirurgisk re-operation för att ta bort implantaten inte blir nödvändig. De kliniska resultaten är ofta goda, men när negativa biologiska händelser, såsom lossning av implantatet, uppstår så påvisas inflammatoriska reaktioner eller så kallade röntgenologiska uppklarningar. De senare antas orsakade av gasfrisättning under nedbrytningen av Mg. Hur kan dessa fynd förenas med den rådande uppfattningen att Mg implantat stimulerar benbildning genom att hämma inflammation och bennedbrytning?

I tre delarbeten i avhandlingen har de biologiska processerna studerats som leder till integrering av Mg implantat i hård- och mjukvävnad. Två typer av Mg implantat studerades, dels så kallade rena (eng. pure) Mg (>99.99 Mg) implantat, dels legerade Mg implantat. Fokus har varit på tidiga inflammatoriska reaktioner samt övergången till vävnadsregeneration. Två experimentella *in vivo* modeller har använts och celler och vävnad har studerats med en kombination av cell- och molekylärbiologiska analysmetoder, ljus- och elektronmikroskopi, Raman spektroskopi samt röntgentekniker.

Den initiala inflammatoriska reaktionen i mjukvävnad och ben orsakad av Mg implantat var kraftigare i jämförelse med icke-nedbrytbara titan (Ti) implantat. Den snabba frisättningen av nedbrytningsprodukter, såsom $Mg^{2+}$ och gas (observerbara som bubblor), skapade en kraftig, men övergående, proinflammatorisk miljö, i vilken cellers genuttryck och secernerade proteiner stimulerades. Bland annat relaterade till kemotaxi, makrofagpolarisation, osteoklastogenes och vaskularisering. Av betydelse var att inga cytotoxiska effekter påvisades. Flera av dessa fynd är i stark kontrast till den gängse uppfattningen att Mg implantat och $Mg^{2+}$ har anti-inflammatoriska effekter.

Därefter minskade inflammationen. Mekanismerna för övergången till en pro-regenerativ fas i både mjukvävnad och ben inbegriper en anrikning av kalcium och fosfor på Mg implantatets yta, en minskning av $Mg^{2+}$ koncentrationen i den lokala, omgivande miljön samt en minskning av gasbildning. Den pro-regenerativa fasen karakteriserades av en förändring av makrofager från pro-inflammatorisk till pro-regenerativ fenotyp, ökad kontakt mellan ben och Mg implantat (ben) och minskad omgivande fibrös kapsel (mjukvävnad).

Av betydelse är att flera av de studerade biologiska processerna var avhängiga de olika nedbrytningsförloppen/hastigheterna hos de två olika typerna av Mg implantat. Rena Mg implantat, som hade en relativt snabbare nedbrytning än legerade dito, hade en närmast omgivande, regenererad benvävnad med annorlunda kemisk sammansättning jämfört med legerade Mg implantat och Ti. För rena Mg implantat påvisades dessutom en tidigare inte beskriven pro-adipogen reaktion i benmärgen. Denna ökade fettansamling var morfologiskt i anslutning

till kvarstående gasbubblor i benmärgen, även relativt långt från övergången mellan implantat och ben. I det sista avhandlingsarbetet visas för första gången att gasbubblor har egenskapen att attrahera celler med proinflammatorisk fenotyp till sin yta samt att cellerna uttrycker ett protein som är inbegripet i avkänning av mekaniska krafter. Dessutom visas för första gången att detta protein uttrycks av celler i gränszonen mellan rena Mg implantat och ben.

Sammanfattningsvis, så visas att Mg implantat genom frisättning av nedbrytningsprodukter förstärker en initial inflammation både i implantat-vävnads gränsskiktet och mer avlägset. Den efterföljande och ändamålsenliga regenerativa fasen är relaterad till materialytans förändring över tid, men kan påverkas negativt av en okontrollerad nedbrytning av materialet. Flera av de (potentiellt negativa) biologiska fynden understryker framtida behov av skräddarsydda materialegenskaper, att öka analysen av biologiska effekter av i synnerhet nedbrytbara material till områden bortanför själva implantat-vävnadsgränszonen samt fortsatt forskning i en klinisk kontext.

# *List of papers*

This thesis is based on the following studies, referred to in the text by their Roman numerals:

I. Ben Amara H, Martinez DC, Shah FA, Johansson Loo A, Emanuelsson L, Norlindh B, Willumeit-Römer R, Plocinski T, Swieszkowski W, Palmquist A, Omar O, Thomsen P.
Magnesium implant degradation provides immunomodulatory and proangiogenic effects and attenuates peri-implant fibrosis in soft tissues
*Bioact Mater 2023; 26:353-369*

II. Ben Amara H, Martinez Dc, Iskhakova K, Emanuelsson L, Norlindh B, Johansson Loo A, Wieland DCF, Zeller Plumhoff B, Willumeit-Römer R, Plocinski T, Swieszkowski W, Shah FA, Palmquist A, Omar O, Thomsen P.
Magnesium implant degradation tunes inflammation and bone repair at the implant interface and beyond
*Submitted for publication*

III. Ben Amara H, Shah FA, Emanuelsson L, Norlindh B, Palmquist A, Omar O, Thomsen P.
Gas bubbles derived from magnesium implants provide mechanosensitive and proinflammatory stimuli in both soft tissue and bone
*In manuscript*

# *Content*

# *Abbreviations*

| | |
|---|---|
| ARG1 | Arginase 1 |
| BCL2 | B-cell lymphoma 2 |
| BSE | Backscattered electron |
| CALCR | Calcitonin receptor |
| CD68 | Cluster of differentiation 68 |
| CEBPβ | CCAAT-enhancer binding protein-beta |
| COL1A | Collagen type I alpha 1 chain |
| CTSK | Cathepsin K |
| DDIT4 | DNA damage inducible transcript 4 |
| EDX | Energy dispersive X-ray spectroscopy |
| ELISA | Enzyme-linked immunosorbent assay |
| FGF2 | Fibroblast growth factor 2 |
| FOXO1 | Forkhead box O 1 |
| ICP–OES | Inductively coupled plasma optical emission spectroscopy |
| IL8 | Interleukin 8 |
| iNOS | Inducible nitric oxide synthase |
| LEPTIN | Leptin |
| MAGT1 | Magnesium transporter 1 |
| MCP1 | Monocyte chemoattractant protein 1 |
| MICRO-CT | Micro-computed tomography |
| MRC1 | Macrophage mannose receptor C type 1 |
| OC | Osteocalcin |
| OPG | Osteoprotegerin |
| PIEZO1 | Piezo type mechanosensitive ion channel component 1 |
| PPARγ | Peroxisome proliferator-activated receptor gamma |
| qPCR | Quantitative polymerase chain reaction |
| RANKL | Receptor activator of nuclear factor kappa-B ligand |
| RUNX2 | Runt-related transcription factor 2 |

| | |
|---|---|
| SAXS | Small-angle X-ray scattering |
| SE | Secondary electron |
| SEM | Scanning electron microscopy |
| SOX9 | SRY-box transcription factor 9 |
| TLR2 | Toll-like receptor 2 |
| TLR4 | Toll-like receptor 4 |
| TNF | Tumor necrosis factor |
| TRPM7 | Transient receptor potential melastatin 7 |
| VEGF | Vascular endothelial growth factor |
| WAXS | Wide-angle X-ray scattering |

# 1. Introduction

Be it injury, infection, or chronic condition, most diseases harm tissues. For millennia, humankind has used materials to replace or augment damaged tissues, while considering both accessibility and ingenuity in their selection. Biomaterials, defined as '*material(s) designed to take a form which can direct, through interactions with living systems, the course of any therapeutic or diagnostic procedure*' [1], are today a mainstay of modern medicine.

However, the demands from biomaterials are high. Not only must they integrate into the accommodating tissues, but they also must restore the tissues' function while preventing infections and treatment failure. Although designed to remain in the body for a lifetime, permanent biomaterials are often removed, even following successful healing, in a variety of clinical scenarios. Of their applications, two continue to spark debates among clinicians, orthopedic and vascular.

## 1.1. WHY IS THERE A *CLINICAL* NEED FOR BIODEGRADABLE IMPLANTS?

In orthopedics, the surgical removal of permanent implants made of stainless steel, cobalt-chromium, or titanium is a routine procedure. For example, in Sweden, approximately 37 000 adults received permanent metallic implants for fracture fixation in 2011, and 13 000 had their implants removed [2]. From 2005 to 2011, the rate of fracture surgeries in adults grew by 20%, while implant removals escalated by 35%, and reached up to 70% for ankle and foot implants. In Germany, more than 175 000 surgical interventions for osteosynthesis implant removal were performed in 2018, meaning that ~80% of osteosynthesis implants were extracted with anticipated costs exceeding 430 million euros per year [3].

Why are permanent implants removed? Certainly, removing these implants is unquestionable when they fail to fulfill their function or in cases of infection [4-6]. However, elective removal of aseptic implants purposed for osteosynthesis is not uncommon and the procedure has been under intense scrutiny [7, 8]. Guidelines for electively removing these implants are often unclear and contradictory. Conflictual recommendations conveyed by expert authorities add ambiguity to the already unclear motivations behind this procedure [7]. Concerns about retaining implants typically relate to late infections, metal toxicity and hypersensitivity, irritation due to implant prominence, corrosion, stress-shielding osteopenia, and neoplasia [7]. Although strongly speculative, all these perceptions are widely echoed by surgeons and have led them to opt for a new operation to extract the implant [7, 9]. An argument frequently used to motivate implant removal, especially in children, is

the potential for the retained devices to complicate future fracture surgeries in adulthood [10].
Such decisions, often guided by risk-seeking behaviors (i.e., to undertake surgery as a preventive measure against loss, therefore accepting the small potential for subsequent issues [11, 12]), come with inherent complications. Infection, wound dehiscence, nerve injury, pain, and refracture rank among the most common complications [8, 13-15] following the removal of metallic osteosynthesis implants, with an overall complication rate of approximately 10% in adult [8, 15] and pediatric patients [13].

In interventional cardiology, endovascular stents are small wire-mesh scaffolds that are routinely introduced with balloon angioplasty to restore the geometry and vasomotion of diseased vessels [16]. Although these implants are intended to be permanent, refractory narrowing of the treated vascular segments (i.e., restenosis) secondary to neointima hyperplasia [17] remains inevitable even in conjunction with the local release of immunosuppressive and antiproliferative agents [18, 19]. Unlike osteosynthesis implants, the interventional disposal of stents is risky, highly complex, and a final alternative in cases of stent infections but not under elective circumstances [20]. One clinical condition that deviates from this principle is the critical congenital coarctation (i.e., narrowing) of the aorta in neonates and infants [21, 22], which necessitates angioplasty in combination with stenting to prevent postoperative collapse of the corrected arterial segment [23]. The efficacy of stenting, although lifesaving, becomes restricted with growth and hinders the development of the treated aorta [23, 24]. Therefore, a surgical revision to longitudinally cut the stent is often needed [23, 24] at the expense of altering the integrity of the vascular walls because of the invasiveness of this intervention [25].

Based on the clinical information detailed above, the permanence of implants used in tissue restoration is not always desired. Biodegradable implants that exert their function and are then eliminated from the body are therefore of high interest and offer the promise of preventing complications posed by permanent devices [26]. In orthopedics, the paradigm of biodegradable implants relies on biomaterials that support the fractured bone at the initial stages of healing and then resorb when osteosynthesis is completed. In interventional cardiology, the paradigm of biodegradable endovascular stents aims to meet the need for immediate vascular geometry restoration and circumvent the late-stage re-narrowing of the stented vessel through biodegradation [27].

In the last decades, synthetic polymers emerged as a biodegradable alternative to nondegradable metallic biomaterials for orthopedic [28, 29] and vascular applications [30]. However, their routine utilization has been challenged by the limitations of their mechanical properties [30, 31]. Attention was drawn by the advent of metallic biomaterials that offered the premise of combining biodegradation with coveted mechanical properties: magnesium (Mg) metallic biomaterials.

## 1.2. MAGNESIUM AS BIODEGRADABLE METALLIC BIOMATERIALS

What are 'Mg metallic biomaterials'? What are not 'Mg metallic biomaterials'? Do all Mg metallic biomaterials degrade? The current literature abounds with biomaterial technologies that incorporate magnesium in their formulation. However, in many instances, these biomaterials are in fact not structurally metallic or they do not have the ability to degrade when in contact with living tissues. Examples of the former group are bioabsorbable polymers [32], bioceramics [33], and hydrogels [34] that are functionalized with Mg in its ionized form to deliver *in situ* $Mg^{2+}$ while dissolving. The latter set of biomaterials includes nondegradable titanium implants that have $Mg^{2+}$ incorporated into their surfaces [35-37]. Both groups, however, lack a core property that sets Mg metallic biomaterials apart: corrosion-driven degradation.

A widely accepted definition of biodegradable metallic biomaterials, whether they are made of zinc, iron, or Mg, is "*metals expected to corrode gradually in vivo, with an appropriate host response elicited by released corrosion products, then dissolve completely upon fulfilling the mission to assist with tissue healing with no implant residues*" [38]. It is clear from this definition that, in addition to corrosion, another component at the core of the concept of biodegradable metals is the host response to the products generated by metallic biomaterial degradation. Therefore, whether a biodegradable Mg metallic implant can fulfill its intended function is highly dependent on both the kinetics of its degradation and the response of the host. In the next paragraph, mechanistic details on the corrosion-based degradation of Mg metallic implants are provided. Further on in the Introduction, the host response is elaborated on in the scope of biocompatibility and bioactivity based on the tissue environment and the constitutive properties of the implants.

### 1.2.1. Degradation mechanisms of Mg metallic biomaterials

All metals can undergo oxidation [39]. For many decades, efforts have been directed toward minimizing the oxidation of permanent implants made of metallic biomaterials such as titanium or stainless steel. Today, oxidation and the resulting corrosion are desired to enable the degradation of metallic implants made of Mg, zinc, and iron.
In the context of implant materials, corrosion is defined by Williams [40] as "*the process of interaction between a solid material and its chemical environment, which leads to a loss of substance from the material, a change in its structural characteristics, or a loss of structural integrity*". This process is, in fact, governed *in vivo* by a succession of anodic and cathodic reactions [38, 41], as illustrated in Figure 1. When in contact with body fluids, the surface of Mg implants immediately reacts by initiating an oxidation process that generates $Mg^{2+}$ and electrons via an anodic reaction. In turn, these electrons are consumed by cathodic reactions, leading to the formation of hydroxides and hydrogen gas. As a consequence of the accumulation of hydroxides, the pH increases and leads to the creation of protective layers atop the implant

surface composed of magnesium hydroxide, $Mg(OH)_2$, and ions that precipitate from the body fluids, mostly calcium and phosphorous [42]. However, this process is somewhat hindered by chloride, which is physiologically abundant in body fluids and can react to form magnesium chloride [38, 41]. The protective layer becomes eroded, and the surface degradation continues, resulting in an ongoing migration of the interface tissue–implant in tandem with the progressive breakdown of the implant [26].

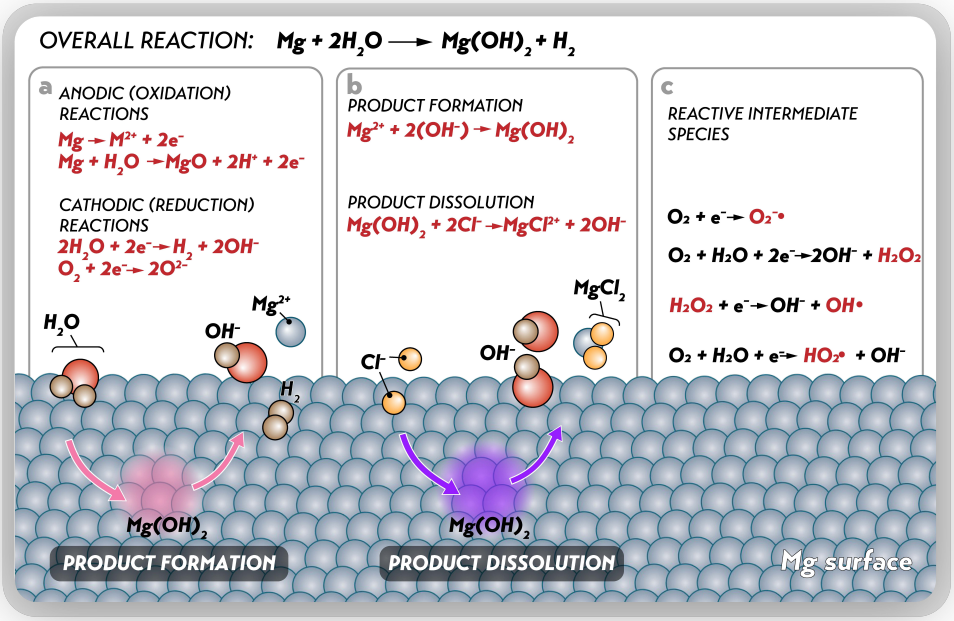


***Figure 1*: Schematic overview of the biodegradation process of magnesium (Mg) metallic biomaterials: a,** Mg degrades via a series of oxidation (anodic) and reduction (cathodic) reactions. Upon oxidation, Mg releases $Mg^{2+}$ in the nearby solution and generates magnesium oxides that passivate the metallic surface. The electrons that are freed and accumulated on this surface are rapidly consumed in the reduction process, primarily by the reduction of water in the biological fluids. **b,** The protective layer rich in magnesium oxide and magnesium hydroxide confers protection to Mg surface, but is fragilized by the high concentration of chloride ions in body fluid. **c,** Although the reduction of water is the main reduction reaction during Mg degradation, a multitude of other reduction reactions can occur producing some of the biologically potent reactive oxygen species that are shown in red such as superoxide ($O_2^{\bullet -}$), hydrogen peroxide ($H_2O_2$), hydroxyl radical ($OH^{\bullet}$), and hydroperoxyl ($HO_2^{\bullet}$). Adapted with permission from [31], Elsevier, and from [26] Springer Nature.

In contrast with other metallic biomaterials [43], a commonly overlooked facet of the degradation of Mg metallic biomaterials is the degree to which reduction reactions shape the corrosion process [44]. As detailed above, many electrons accumulate at the metal surface upon Mg oxidation. These are quickly used up by the balancing reduction reactions that involve mostly water and oxygen (but also other biological molecules; for instance, by reducing the metal ions in metalloproteins) to release hydrogen gas and hydroxides. However, these are not the sole products of these reduction reactions. Reactive oxygen species (such as hydroxyl radicals, hydroperoxyl, hydrogen peroxide and superoxide), as well as reactive nitrogen species, are also generated at the implant surface [44] and therefore might also contribute to the biological response of the interfacing tissues.

### 1.2.2. 'Biodegradable', 'bioresorbable', or 'bioabsorbable'?

Notably, this corrosion-driven degradation of metallic biomaterials, including Mg, is inherently different from that of other degradable biomaterials, such as polymers or bioceramics. Polymer degradation involves hydrolysis and cell-mediated enzymatic breakdown [26], while bioceramic degradation relies on dissolution and disintegration [45]. Irrespective of their degradation mechanisms, all these biomaterials are interchangeably designated '*biodegradable*', '*bioresorbable*' and '*bioabsorbable*' [46]. In the present thesis, only the term '*biodegradable*', most often used to refer to metallic biomaterials that undergo degradation in biological systems, is employed for clarity.

### 1.2.3. Degradation of pure *versus* alloyed Mg: material development in advance

Based on the definition presented earlier, biodegradable metallic biomaterials – including Mg – principally fall into the following two groups [38]: 1. *Pure metals* that are composed of a single metallic element and possess impurities at levels below commercial tolerance thresholds; and 2. *Biodegradable alloys* that are formulated with one or more alloying elements in carefully adjusted quantities.
The use of pure Mg has attracted long-lasting interest in implants aimed at treating injuries and diseases of the soft tissue [47] and bone [48] since early clinical reports dated before 1900 [49]. However, the following two major drawbacks prevented the wide clinical utilization of pure Mg: elevated levels of impurities and weak mechanical properties [38, 41]. Remnant impurities (such as iron, nickel, and copper) are unavoidably incorporated during the fabrication of pure and alloyed Mg biomaterials. During corrosion, they form local cathodic sites that deeply accelerate the degradation process [41]. By controlling the levels of impurities, the degradation rate of pure Mg may diminish 1000-fold [50].

Alloying is another approach to tailoring degradation. The advent of new possibilities for alloying Mg into various formulations enabled the design of metallic Mg implants that are currently implemented in clinical practice. This new

generation of Mg implants benefits from enhanced mechanical performance and controlled degradation behavior based on the refined microstructure and optimized material processing. Some examples include rare-earth (mostly yttrium and neodymium)-based Mg alloys and Mg-Zn-Ca alloys, which are currently employed with success as osteosynthesis implants [51-53] and endovascular stents [54] in patients.

## 1.3. ARE MAGNESIUM METALLIC BIOMATERIALS BIOCOMPATIBLE?

The human body is not a habitat that one would perceive as hospitable for an implanted biodegradable metal. From a pure corrosion science perspective, it might be regarded as 'fluids' containing saline electrolytes with elevated levels of highly corrosive chlorides, enriched with oxygen, a pH near 7.4, and a temperature of 37°C [41]. This minimalistic perception of the *in vivo* systems indeed guided much of the initial *in vitro* work that was dedicated to predicting how Mg metallic biomaterials behave when in contact with living tissues [50, 55, 56]. In recognition of the complexity of living systems, varieties of cells and/or proteins were then incorporated into *in vitro* set-ups with the purpose of better anticipating not only Mg biomaterial performance but also host response [57, 58]. Many of these studies were tailored to satisfy the requirements of regulatory bodies that evaluate their biological 'safety', particularly the traditional ISO 10993 series [58, 59]. According to this standard, extracts obtained by pre-degrading a substrate of pure or alloyed Mg (or any other biodegradable material) in an *in vitro* medium are administered to cells at different concentrations to measure cytotoxicity, typically after 72 h and at 37°C. This holds some logic if it is assumed that these tests enable investigation of the effects of end byproducts such as $Mg^{2+}$ and hydroxides on cells. However, these extracts do not contain the other very short-lived yet essential components produced *during* the Mg degradation process, such as hydrogen and other reductive species [44]. Therefore, can *in vitro* testing be considered valid to assess whether Mg metallic biomaterials are 'biocompatible'?

### 1.3.1. *In vitro versus in vivo*: the contradictory conundrum

An answer to this question may reside in the growing concerns about contradictory results from *in vitro* and *in vivo* testing of Mg metallic biomaterials [59, 60]. Instances where the same Mg metallic biomaterial is reported to be cytotoxic *in vitro* (i.e., cell viability lower than 75% according to ISO 10993-5) but successfully integrates into tissues (i.e., osseointegration herein) *in vivo* are manifold [61-65]. The same group of *in vitro* studies also showcases how the viability of cells of different types might profoundly differ when testing the same Mg biomaterial. These contradictions stem, at least in part, from the elevated $Mg^{2+}$ concentrations and high alkalinity *in vitro* that inevitably lead to pronounced cytotoxic effects [58, 59]. Diluting Mg degradation extracts then becomes an accepted and recommended trade-off [58, 59]. However, does this make *in vitro* tests more relevant to evaluate Mg metallic biomaterial biocompatibility?

### 1.3.2. Biocompatibility of degradable *versus* nondegradable biomaterials

Biocompatibility is defined as *'the ability of a material to perform with an appropriate host response in a specific application'* [1, 66]. Here, the 'host' is more than just a mere saline solution but a complex combination of a 'solution' with anions and cations and an assortment of large, chemically reactive molecules and cells that can be in quiescent or dynamic states. The biocompatibility process inherently includes some degree of trauma to the accommodating tissues during the introduction of the implant and is most accurately depicted *in vivo* [67, 68]. Initial biocompatibility studies using *in vivo* models largely focused on nondegradable biomaterials to demonstrate the structural and functional 'stable equilibrium' without adverse effects occurring between the host and the biomaterial, often for intermediate or long durations [68]. These studies were thereafter transposed with considerable analogy to investigate the biocompatibility of host–degradable biomaterials, including Mg. However, the fundamental differences between the two biomaterial groups are often overlooked, leading to an incomplete understanding of the biocompatibility of Mg metallic biomaterials.

To provide a clearer picture, let us look at a metallic osteosynthesis implant used to secure the fixation of a fracture, as shown in Figure 2. First, to put into the context of the interaction with the host, a nondegradable implant would not be subject to structural or chemical alterations when introduced to living tissues. In contrast, biodegradation is immediately initiated upon the implantation of a biodegradable Mg metallic biomaterial. The degradation changes the topography, area, and chemistry of the implant surface and alters the quality of the host–implant interface [26, 67]. Therefore, it might be perceived that these sudden changes potentiate the initial inflammatory response of the interfacial tissues to the biodegradable implant. Second, as the implant undergoes degradation, the released byproducts are presented continuously to the accommodating tissues, a scenario not seen with nondegradable implants. The resulting interplay between the biodegradable implant and the host is therefore dynamic and evolves from the onset of inflammation through the subsequent phases of tissue repair [67].
Thus, biocompatibility and biodegradability are opposite polar extremes when considering the spectrum of properties of system host–biodegradable implants. Implants that degrade vigorously release degradation byproducts, thus impeding biocompatibility, and vice versa [39, 50]

### 1.3.3. Biocompatibility of biodegradable implants: location matters

An implant may simultaneously interface with bone and with overlaying soft tissues (Figure 2). A scenario where a biodegradable implant is in contact with adjacent tissues that hold different functionalities is common [69]. Therefore, how do different microenvironments influence the behavior of biodegradable implants and the response of tissue?

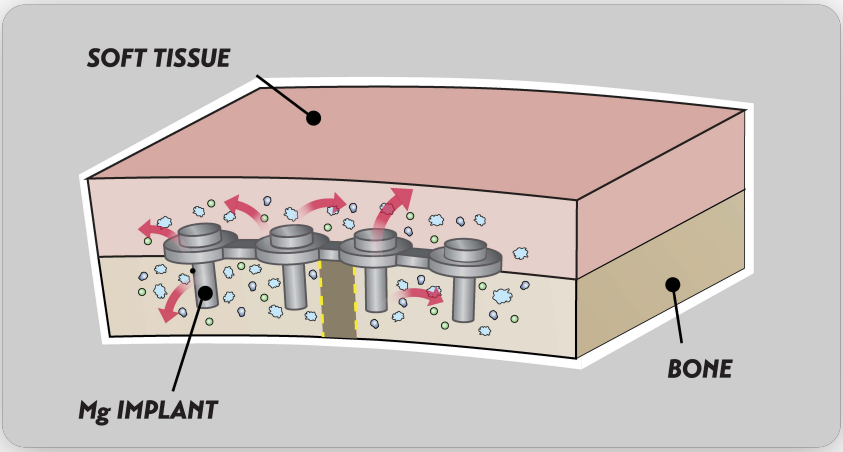


***Figure 2*: A magnesium metallic implant, for fracture osteosynthesis, that simultaneously interfaces with soft tissue and bone**. The degradation products are released to their milieu and elicit a cellular response that might be tissue-dependent.

Nature uses gradients in the properties of adjacent yet different tissues through subtle adjustments of their composition and structure [70]. These differences distinctly shape the interaction between biodegradable Mg metallic implants and adjacent tissues such as bone and soft tissues. In the bone environment, new bone deposition in direct contact with the implant surface has been consistently reported [53, 71]. In soft tissue, a handful of studies indicate that a fibrous capsule that is deposited around the implant surface denotes the late-stage response to metallic Mg biomaterials [72]. However, biodegradability and biocompatibility are not constitutive properties of these biomaterials but rather contextual to specific environmental cues [67]. Restricting the biocompatibility of metallic Mg implants to the morphological definition of a collagenous capsule (in soft tissues) or a mineralized deposition (in bone) that conformally surrounds the implant is insufficient. Assessing the immune response coupled with these late-stage tissue responses depends on the nature of the tissue milieu, which is necessary to determine biocompatibility.

## 1.4. ARE MAGNESIUM METALLIC BIOMATERIALS BIOACTIVE?

'Bioactive materials' is nothing but a widespread designation given to Mg metallic biomaterials in the literature. However, before delving into the relevance of this appellation, what is a bioactive material?

The term bioactivity finds its roots in the duality with the early concept of biomaterial 'inertness', i.e., a material that generates a minimal tissue response; although it might be argued that some interaction always occurs at the interface between the living tissues and biomaterials [73]. According to Hench [74], '*a bioactive material is one that elicits a specific biological response at the interface of the material which results in the formation of a bond between the tissues and the material*'. This definition, introduced more than 40 years ago, was mostly ascribed to biomaterials (such as ceramics) that create an environment compatible with osteogenesis and that form a mineralized bond at the interface with living tissues. A more recent definition that captures a wider spectrum of biological activities beyond bone growth was provided by Williams [73] as follows: '*a biomaterial that beneficially and appropriately directs interactions between the device and the host system through the modulation of biological activity*'. Therefore, the alteration of biological activity must be intentional to recognize a given biomaterial as 'bioactive'. In terms of biocompatibility, bioactivity is not an innate characteristic of the biomaterial but rather a property of the system host–biomaterial.
Under this definition, Mg metallic biomaterials are presumed to primarily modulate the following three biological processes: inflammation, tissue repair/regeneration, and cancer growth. The first two activities will be discussed below, while readers interested in the third process should reference a previous review [75].

### 1.4.1. Magnesium metallic biomaterials and the immune response

The capacity to attenuate local inflammation has traditionally been attributed to Mg metallic biomaterials [76, 77]. This viewpoint has been solidified by an ever-increasing number of epidemiological, experimental, and clinical studies on the impact of $Mg^{2+}$ homeostasis derangement.
On the one hand, low dietary $Mg^{2+}$ intake and hypomagnesemia are recognized as contributors to the pathophysiology of numerous diseases, including diabetes [78], cancer [79], infection [80], cardiovascular diseases [81], and inflammatory disorders [82]. Elevation of the inflammatory response and oxidative stress in animals and humans has been associated with low serum concentrations of $Mg^{2+}$ [83]. Several clinical studies have reported that the marker of chronic inflammation, C-reactive protein (CRP), is elevated in subjects with low Mg intake, often in association with type 2 diabetes [84]. High serum levels of the inflammatory cytokines tumor necrosis factor (TNF) in obese individuals [85] and interleukin 6 (IL6) in diabetic patients correlate [78] with a low serum concentration of $Mg^{2+}$. On the other hand, in many of the pathological settings described above, the administration of $Mg^{2+}$ is effective in attenuating inflammation [86] and for potentiating the immune response to infection [87] and cancer [88]. $Mg^{2+}$ is routinely used in obstetric practice to suppress preterm labor [89] via a decrease in TNF and IL6 production mediated by the regulation of the nuclear factor κB (NF-κB) inflammatory pathway [90]. The wide spectrum of $Mg^{2+}$ activity stems from its key role in a myriad of basic biological mechanisms, particularly enzymatic reactions required for protein synthesis and energy metabolism [91].

This compelling evidence that supports the fact that $Mg^{2+}$ supplementation alleviates inflammation has fueled efforts to demonstrate that locally released $Mg^{2+}$ from metallic Mg implants can also have an anti-inflammatory benefit. Indeed, results from numerous *in vitro* studies indicate that the degradation of pure or alloyed Mg metallic biomaterials attenuates the inflammatory response mostly in monocyte/macrophage lines [92-96]. The promotion of anti-inflammatory/prohealing macrophages (M2 – alternatively activated) in conjunction with the suppression of proinflammatory macrophages (M1 – classically activated) has been suggested as part of the mechanism [94-96].
However, when examining these findings, one must account for the fact that cells are challenged with degradation extracts from tested Mg implants. Not infrequently, these Mg degradation extracts, which lack most of the reduction reaction products such as hydrogen and reactive oxygen species (ROS) [44], are subjected to multiple dilutions to avoid hampering the viability of the cells. With this in mind, there is no denying that the relevance of these *in vitro* outcomes to living tissues is questionable.

So, what do preclinical and clinical studies tell us?
Findings from clinical trials of up to 3 years on Mg-based biodegradable stents do not link the reported adverse effects to any inflammation caused by stent degradation [97-99]. Recent systematic reviews suggest that the absence of clinically discernible symptoms in patients is typical at 12-month follow-ups after metallic Mg implantation for osteosynthesis [100, 101]. However, initial inflammation of soft tissue near Mg osteosynthesis implants is not uncommon and is reportedly associated with subcutaneous gaseous cavities due to implant degradation [102-106]. In most instances, this initial inflammation of soft tissue subsides when osteosynthesis is achieved. However, when Mg implant failure occurs, the uncontrolled response in soft tissue persists [107]. Importantly, the persistence of soft tissue inflammation in conjunction with the failure of orthopedic metallic implants is well documented with the use of nondegradable cobalt-chromium [108], which releases ions and micron-meter-sized particles that are cytotoxic to macrophages and leads to an aberrant fibrotic response [109].
These clinical events challenge the anti-inflammatory activity of Mg metallic biomaterials and underscore the necessity to understand the mechanisms through which the degradation of metallic Mg implants regulates inflammatory pathways in adjoining tissues, including soft tissue and bone.
However, surprisingly, *in vivo* exploration of the initial inflammatory window following the implantation of Mg metallic biomaterials has been largely overlooked in preclinical trials [110]. An exception is one study that demonstrated that hydrogels releasing $Mg^{2+}$ beyond the initial 7 d post-implantation prolong inflammation and hinder bone formation [111]. Considering that metallic Mg implants deliver a complex combination of degradation products that surpass the simplistic local release of $Mg^{2+}$, understanding the regulation of the local inflammatory reaction and its influence on metallic Mg implant biocompatibility in soft tissue and bone is essential.

### 1.4.2. Magnesium metallic biomaterials and tissue repair/regeneration

Given their primary use in orthopedic applications, the ability of Mg metallic biomaterials to encourage bone growth has drawn significant attention [77]. But are all biomaterials that promote bone formation bioactive?
If bioactivity relates to the formation of new bone at the implant surface, biomaterials that are known as 'bioinert' will erroneously fall into the bioactive category. One such biomaterial is gold, which aids bone formation to some degree [112]. Then, what sets apart an osteo-promotive bioactive material?
A reasonable mechanism that confers bioactivity to Mg metallic biomaterials is the release of degradation products [73]. Among these, $Mg^{2+}$ is known for its ability to modulate the pathways of bone anabolism and catabolism.

Indeed, a plethora of *in vitro* studies using a variety of cell types [mesenchymal stem cells (MSCs) [113-116], osteoblasts [117], and osteoclast precursors [118, 119]] provide evidence that $Mg^{2+}$ or extracts (under different dilutions) from the degradation of Mg metallic biomaterials encourage bone formation via the following two mechanisms: 1. *by promoting osteogenesis*, which involves the activation of the canonical Wnt/β-catenin signaling pathway that favors MSC osteogenic differentiation [113, 115], often in tandem with the action of the neuropeptide calcitonin gene-related polypeptide-α (CGRP) [120, 121]; and 2. *by arresting osteoclastogenesis* via the suppression of the receptor activator of nuclear factor κB ligand (RANKL) –NF-κB – nuclear factor of activated T cells 1 (NFATc1) axis [119]. Beyond this osteo-promotive action, another set of *in vitro* studies also showed the proangiogenic effect of $Mg^{2+}$ or Mg degradation extracts in MSCs and endothelial cells [122-124].

There is no doubt that the available preclinical and clinical data support the notion that metallic Mg implants foster bone growth [53, 71, 120, 125], angiogenesis [123], and osteosynthesis success [51-53]. This concept of promoting repair and regeneration processes has also proven true in animal and human vascular tissues that are treated with biodegradable Mg stents [54, 126].
It is, however, questionable to infer the cellular mechanisms that drive these restorative outcomes and their desired concentrations of Mg degradation products only from *in vitro* studies. For example, the widespread thesis that metallic Mg implants reduce osteoclastogenesis is mostly built upon findings from *in vitro* experiments where osteoclast precursors are exposed to $Mg^{2+}$ or diluted Mg degradation extracts. However, these cells do not encounter other degradation products, such as some reductive species, nor do they interact with other cell types (such as immune cells or osteoblasts) that might alter their behavior. ROS are potent activators of osteoclast differentiation and activity, and in an *in vivo* environment, with excess ROS, one would speculate that osteoclasts would be stimulated and not abrogated. Moreover, assuming that metallic Mg implants would reduce osteoclastic activity, would that impair the bone remodeling process? Above all, beyond the promotion of bone growth, does the degradation of metallic Mg implants also affect the quality of the interfacial bone [127]? It is evident that a

mechanistic understanding of the cellular regulation of the processes of tissue repair and regeneration in response to metallic Mg implants *in vivo* is needed. Equally important is the characterization of the functional competence of the newly formed tissues.

## 1.5. THE ENIGMA OF GASEOUS CAVITIES AROUND MAGNESIUM IMPLANTS: *HORROR VACUI* OR PARTNERS IN REPAIR?

A particular debate is presently stirring conversation among medical radiologists [128]: that is how to interpret radiolucent cavities of the soft tissue and the bone marrow that are seen in patients with Mg osteosynthesis implants [129-131]. To the untrained eye, these atypical radiographic features might be misinterpreted as a postsurgical infection or as an implant loosening [128], yet they indicate the accumulation of gas that has been released from Mg implants [38].

In fact, once a metallic Mg implant is in contact with tissues, the degradation products do not remain confined to the implant–tissue interface. By generating one mole of hydrogen from each mole of Mg, 5 g of a metallic Mg implant releases an estimated 236 ml of hydrogen gas per day (which corresponds to 40 ml/cm$^2$/day) [132]. Therefore, substantial amounts of hydrogen can diffuse to the interfacial tissues and beyond. Morphologically, gaseous pockets become evident in tissues, typically in the initial months following implantation [100]. However, how these cavities influence the tissue response remains unclear.
It is widely accepted that hydrogen gas has a large array of beneficial effects [133], such as the suppression of inflammatory cytokines [interleukin 1β (IL1β), IL6, and TNF] [134], the inhibition of apoptotic factors (caspase-3, caspase-8, and caspase-12) [134] and acute oxidative stress (by neutralizing ROS) [133], and the promotion of angiogenesis [by the activation of vascular endothelial growth factor (VEGF)] [135]. More than one century ago, hydrogen released from metallic Mg seeds was reported to treat vascular deformities [136] by eliciting thrombosis and fibrotic transformation, thereby leading to their regression [137, 138].

However, these favorable effects are hard to reconcile with the pronounced inflammation associated with the gaseous pockets in tissues near failing metallic Mg implants in patients [102, 105]. Gas accumulation is thought to hinder implant healing [72], advocating even the removal of gaseous voids by puncture procedures in clinical [49] or preclinical settings. Moreover, evidence indicates that hydrogen is present in small fractions inside the gaseous pockets [139, 140] and the level substantially declines with time due to its rapid diffusion depending on the nature of the tissue [141], with no alteration of the cavities' morphology [139].
Therefore, characterizing the *in situ* cellular response to the gaseous pockets is necessary to better predict the fate of tissues surrounding these entities at the interface of the Mg implant and at remote distances. By remotely diffusing from the tissue–implant interface, degradation products from Mg or other metallic implants can engage deeply into the surrounding tissues [142] such as the bone

marrow [143]. Determining the response in these remote sites is equally important to determining that at the tissue–implant interface.

# *2. Aims*

This thesis is intended to (1) investigate the modulation of the initial inflammatory response by the degradation of magnesium (Mg) implants at their immediate tissue milieu and (2) determine the role of the interconnection between *cellular response–implant degradation* at the inflammation stage in guiding subsequent repair and regeneration, leading to the integration of Mg implants into different tissues.

The specific aims of each paper included in this thesis are as follows:

- To determine whether the sequential release of degradation products from Mg implants amplifies inflammation and cytotoxicity in the tissue microenvironment and increases fibrotic encapsulation compared to nondegradable titanium implants in a rat soft tissue model (Paper I).

- To study how different degradation behaviors by two Mg implants influence inflammation at the bone-implant interface and beyond and to compare their osseointegration with that of nondegradable titanium implants in a rat bone model (Paper II).

- To investigate the role of gas cavities generated *in situ* by Mg implant degradation in modulating local cellular processes, including inflammation and mechanosensation, and in steering tissue assembly in rat models of soft tissue and bone (Paper III).

# *3. Materials and Methods*

## 3.1. BIOMATERIALS & ANIMAL MODELS

### 3.1.1. Implants & biomaterials

Disc-shaped implants (*thickness* = 1.4 mm, *diameter* = 9 mm) and screws (*length* = 2.3 mm, *diameter* = 2 mm) were used for implantation in soft tissue and bone, respectively.

- *Biodegradable magnesium (Mg)-based biomaterials* used for implant fabrication consisted of high-purity Mg (≥99.995%) and a Mg alloy (MgYREZr – 4% yttrium, 3% rare earth elements – WE43 alloy family). While the pure Mg employed herein is only intended for experimental purposes, the MgYREZr alloy has been approved for clinical applications and is used in orthopedic implants, for example.
- *Nondegradable titanium* served as a control biomaterial in this work. Commercially pure titanium (Grade 4) was employed to fabricate control implants.

Disc-shaped implants composed of pure Mg and titanium were used in Paper I, whereas screw-shaped implants fabricated from pure Mg, alloyed Mg, and titanium were used in Paper II. Paper III investigated disc- and screw-shaped implants of pure Mg. In addition, disc-shaped implants composed of pure Mg (Paper I, Paper II) and alloyed Mg (Paper II) were needed for *in vitro* immersion tests.

### 3.1.2. Animal models

Male Sprague Dawley rats, aged ~ 12 weeks (Taconic Biosciences), were used in all *in vivo* studies in the present work. Animal experimental procedures, however, were carried out using different approaches depending on the implantation site, i.e., in soft tissue or bone. Each animal received only one implant material type. All animal experiments in Paper I, Paper II, and Paper III were conducted after approval from the Local Ethical Committee for Laboratory Animals at the University of Gothenburg, Sweden (Dnr-14790/2019 & Dnr-02437/2018). The animal models, targeted anatomical sites, implant materials, and their design specificities are summarized in **Table 1**.

***Table 1.*** *Overview of the animals, anatomical location, implant materials, and implant designs employed in this thesis.*

| ***Papers*** | ***Species*** | ***Sex*** | ***Anatomical location*** | ***Biomaterials*** | ***Implant design*** |
|---|---|---|---|---|---|
| ***I*** | Rat (SD) | Male | **Dorsum** subcutis | **Titanium** (Grade 4)<br>**Pure Magnesium** | Disc-shaped |
| ***II*** | Rat (SD) | Male | **Tibia** distal metaphysis | **Titanium** (Grade 4)<br>**Pure magnesium**<br>**Alloyed magnesium** (MgYREZr) | Screw-shaped |
| ***III*** | Rat (SD) | Male | **Dorsum** subcutis &<br>**Tibia** distal metaphysis | **Pure magnesium** | Disc-shaped &<br>Screw-shaped |

***SD****:* Sprague Dawley

***Soft tissue*** − In addition to enabling '*classical*' biocompatibility testing, the present model permits detailed characterizations of the cell-implant interaction in a spatiotemporal fashion via a suite of cellular, molecular, and structural analyses. The soft tissue model was employed in Paper I and Paper III.
In brief, animals were anaesthetized by isoflurane inhalation, and their backs were shaved and cleaned. Incisions were executed to bluntly dissect subcutaneous pockets that received disc-shaped implants or were left without implants (*sham*). After the pocket was closed with sutures, analgesic medication was administered immediately and 8 h postoperatively. Animals were then sacrificed with an overdose of pentobarbital after 1, 3, 6, 14, or 28 d. The following types of samples were retrieved according to the following sequence:

1. *implants*: collected upon pocket reentry.
2. *peri-implant exudates (and sham exudate)*: once implants were retrieved, pockets were washed using Mg-free Hanks' Balanced Salt Solution (HBSS). No sham exudates were collected at 14 d and 28 d due to wound closure.
3. *peri-implant tissue (and sham tissues)* or 4. *implant and peri-implant tissue en bloc.*

***Bone*** − The bone model utilized in Paper II and Paper III allows the characterization of osseointegration, typically observed 4 weeks after a titanium implant is inserted; in addition, the earlier inflammatory response can be investigated.
In short, under isoflurane anesthesia complemented by local lidocaine infiltration, the metaphyseal bone of the left and right tibia was exposed following incision, reflection of the overlying skin and muscle upon incision, and dissection of the periosteum. One bone defect was drilled under saline irrigation to monocratically implant one screw in each tibia. The superficial layers were repositioned and sutured, and analgesics were administered immediately and postoperatively at 8 h.

After 3 d and 28 d, the animals were sacrificed with pentobarbital overdose, and the following types of samples were collected:

1. *implants*
2. *peri-implant bone*: retrieved by trephination
3. *implant and peri-implant en bloc.*

## 3.2. PREPARATION OF BULK SAMPLES

Implants and associated tissues (soft tissues in Paper I and Paper III, bone in Paper II and III) were fixed in formalin, dehydrated, and embedded in plastic (LR White). Micro-CT analysis was then used to image implant and peri-implant bone (Paper II and Paper III). To obtain sections for histology, each plastic-embedded sample was sawed in two hemi-blocs, one of which was used to prepare a central ground section (~20 µm thick).
Additional samples consisting of peri-implant tissues (soft tissues in Paper I and Paper III, bone in Paper II and III) were collected following implant retrieval. Prior to the preparation of a central section (~5 µm thick), all tissues were formalin-fixed, dehydrated, and embedded in paraffin. Bone samples were subjected to ethylenediaminetetraacetic acid EDTA decalcification after their fixation in formalin to enable sectioning.

***Resin-cast etching*** – To visualize the lacuno-canalicular network of osteocytes through electron microscopy in Paper III, the polished surface of the hemi-blocs of the plastic-embedded implant and neighboring bone were treated in sequence with orthophosphoric acid (to remove the organic components) and sodium hypochlorite (to remove the inorganic components). Electron microscopy imaging of the remaining resin filled at the sample surface was then performed.

## 3.3. HISTOLOGY & IMAGE ANALYSIS

### 3.3.1. Histology

In the present work, sections of tissues fixed in formalin and embedded in plastic or paraffin were stained. Qualitative histological examination of soft tissue and bone, as well as histomorphometric analyses, were performed.
Nondecalcified ground sections from tissues embedded in plastic were stained with toluidine blue (Paper I, Paper II, and Paper III) and methylene blue-basic fuchsin (Paper II, and Paper III).
Toluidine blue and methylene blue are basic thiazine dyes that preferentially stain acidic components of tissues and exhibit a high affinity to the nuclear material in tissue. The acidophilic properties of these dyes allow them to stain components of the extracellular matrix at different intensities. For example, in Paper II and Paper

III, 'younger' bone (i.e., recently formed bone) has a higher content of acid phosphate groups and generates darker stains than 'older' bone. This color contrast in the bone matrix can be increased by combining methylene blue with basic fuchsin, which has an alkaline affinity.
Toluidine blue and methylene blue also possess metachromatic properties and thus selectively produce a different color in specific tissue components. For instance, metachromasia is obtained when these dyes react with glycosaminoglycans in mast cell granules. The display of a distinct purple or red color allows the identification of mast cells in soft tissue (Paper I) and in bone (Paper II).
Sections from decalcified (if mineralized, i.e., bone) paraffin-embedded tissues were stained with hematoxylin and eosin (Paper I, Paper II, and Paper III). When combined with metallic cations – typically aluminum – hematoxylin exhibits a high affinity for anionic nucleic acids and stains the nuclear material a characteristic purple/blue color. In contrast, eosin, by staining cationic proteins, causes the cytoplasm and extracellular matrix components to appear in various shades of pink under light microscopy. Moreover, due to the fluorescent property of eosin (which displays green emission under blue or green excitation), eosin (but not hematoxylin)-stained components can be selectively examined under fluorescence microscopy, as described in Paper I.
Histology and histomorphometry were also performed on cytospin preparations stained with May Grünwald-Giemsa. By combining methylene blue and eosin, this stain best distinguishes the nuclei and cytoplasm of leucocytes from erythrocytes. Thus, as reported in Paper I, polymorphonuclear cells could be detected and counted in cytospin slides prepared from exudate samples.

### 3.3.2. Image analysis

Histomorphometry in Paper I, Paper II, and Paper III was performed with brightfield full-slide scans (pixel size = 0.43 µm) acquired using a light microscope (Nikon Eclipse 600) and a 20x objective (Plan Apo 20×/0.75). Most of the histomorphometry metrics in the present work were semiautomatically quantified using the image analysis software Qupath. This open-source application is dedicated to the visualization and quantitative analysis of 2D multichannel full slide images (>30 000 pixels in x,y), unlike other popular image analysis software, such as ImageJ. Through Qupath built-in algorithms, tissues and cells can be detected and classified depending on the presence of specific markers in addition to the calculation of intensity, distance, and shape features.
In Paper I, for example, the Qupath workflow included the processing of full-slide images of soft tissue sections stained with hematoxylin and eosin using color deconvolution (i.e., the decomposition to single absorbance values of each hematoxylin and eosin, separately). Then, hematoxylin-stained nuclei were segmented to detect cells and measure their density relative to the area of the regions of interest.
Based on a comparable workflow, 'positive cell detection' is another built-in command that was used in Paper I, Paper II, and Paper III to quantify the relative

density of cells immunoreactive to targeted proteins (among several thousand included cells) in full slide scans of immunohistochemistry sections.
Custom algorithms with or without deep-learning-based extensions (such as StarDist) were also used in Paper II and Paper III to segment bone marrow and study its cellular morphology and composition.
Few other metrics were measured manually on full slide images, such as the thickness of the peri-implant fibrous capsule in Paper I, bone-implant contact and bone area between threads in Paper II, and the density of mast cells in the peri-implant tissues in Paper I and Paper II, as well as the size and shape of voids associated with Mg-based implants in Paper III.

## 3.4. CELLULAR & MOLECULAR BIOLOGY METHODS

### 3.4.1. Gene expression – *qPCR*

Quantitative polymerase chain reaction (qPCR) is the gold standard for the quantification of nucleic acid molecules in biological samples. The technology provides information regarding the quantity of specific transcripts in a cell or tissue. qPCR analysis comprises a combination of the following steps: 1) isolation of RNA from target cells/tissue; 2) reverse-transcription of mRNA to cDNA; 3) amplification of a segment of interest of the cDNA using PCR; and 4) detection and quantification of the selected transcript. Although the methodology is generally simple, numerous steps and reagents must be optimized and validated to minimize the variability and maximize the quality of the results.
In Paper I and Paper II, a variety of genes were targeted (**Table 2**) for qPCR analysis in biological samples of different natures, including the following:

- *Cells adherent to the implant* surface in Paper I and Paper II were detached from the bearing implant surface into RNA preservation medium (DNA/RNA shield®) using a plate shaker.
- *Peri-implant exudate*, in Paper I, was harvested by lavage of the tissues adjoining the implant upon its collection (washing with a Mg-free HBSS solution). Cells in the exudate were then pelleted and transferred to RNA preservation medium. Identical procedures were applied for exudates from sham sites in Paper I.
- *Peri-implant tissue* consisted of soft tissues in Paper I and bone in Paper II and was retrieved in a standardized fashion through soft tissue punches or bone trephines. The samples were then homogenized by mechanical disruption through high-speed shaking with stainless-steel beads (TissueLyzer®) into RNA preservation medium. Sham tissues in Paper I were subjected to the same procedures.

Prior to reverse transcription of mRNA to cDNA, total RNA was extracted from all lysates used for qPCR via spin-column-based isolation and purification. PCR was then conducted using prevalidated gene-specific primers, followed by the normalized quantification of the targeted mRNA transcripts relative to reference genes that were screened and validated beforehand (GeNorm, Normfinder). Pilot

***Table 2.*** *Panels of targeted genes and reference genes in Paper I and Paper II with information on related biological processes.*

| *Papers* | *Targeted genes* | *Related biological processes* | *Reference genes* |
|---|---|---|---|
| ***I*** | ***Tnf, Il8, Mcp1*** | cytokines/chemokines | ***GAPDH*** |
| | ***iNos, Mrc1*** | macrophage polarization | |
| | ***Vegf*** | neoangiogenesis | |
| | ***Fgf2, Foxo1*** | fibrogenesis | |
| | ***Ddit4, Bcl2*** | apoptosis | |
| | ***Tlr2, Tlr4*** | TLR pathways, inflammation | |
| | ***Trpm7, Magt1*** | $Mg^{2+}$ channels | |
| ***II*** | ***Tnf, Mcp1*** | cytokines/chemokines | ***HPRT1*** |
| | ***iNos, Mrc1*** | macrophage polarization | |
| | ***Vegf*** | neoangiogenesis | |
| | ***Col1a, Foxo1*** | tissue regeneration | |
| | ***OC, Runx2,*** | osteogenesis | |
| | ***Ctsk, Calcr, Rankl, Opg*** | osteoclastogenic regulation | |
| | ***Cebpβ, Leptin, Pparγ*** | adipogenesis | |
| | ***Sox9*** | chondrogenesis | |
| | ***Piezo1*** | mechanotransduction, ion channel | |
| | ***Trpm7*** | $Mg^{2+}$ channel | |

***Tnf***: Tumor necrosis factor; ***Il8***: Interleukin 8; ***Mcp1***: Monocyte chemoattractant protein 1; ***iNos***: Inducible nitric oxide synthase; ***Mrc1***: Macrophage mannose receptor C type 1; ***Vegf***: Vascular endothelial growth factor; ***Fgf2***: Fibroblast growth factor 2; ***Foxo1***: Forkhead box O 1; ***Ddit4***: DNA damage inducible transcript 4; ***Bcl2***: B-cell lymphoma 2; ***Tlr2***: Toll-like receptor 2; ***Tlr4***: Toll-like receptor 4; ***Trpm7***: Transient receptor potential melastatin 7; ***Magt1***: Magnesium transporter 1; ***Col1a***: Collagen type I alpha 1 chain; ***Oc***: Osteocalcin; ***Runx2***: Runt-related transcription factor 2; ***Ctsk***: Cathepsin K; ***Calcr***: Calcitonin receptor; ***Rankl***: Receptor activator of nuclear factor kappa-B ligand; ***Opg***: Osteoprotegerin; ***Cebpβ***: CCAAT-enhancer binding protein-beta; ***Leptin***: Leptin; ***Pparγ***: Peroxisome proliferator-activated receptor gamma; ***Sox9***: SRY-box transcription factor 9; ***Piezo1*:** Piezo type mechanosensitive ion channel component 1.

soft tissue (Paper I) and bone (Paper II) trials were used to verify RNA quality, RNA concentration, and possible inhibition occurring at the reverse-transcription or PCR steps.

### 3.4.2. Cell counting and cell viability

Fluorescence-based automated cell counting with *NucleoCounter* uses a fluorescent dye, i.e., propidium iodide, to stain and automatically detect cell nuclei, irrespective of the cell size or morphology.
First, the cell suspension is mixed with lysis buffer (*Reagent A*) to disrupt the plasma membrane of cells, making nuclei amenable to fluorescence staining. A stabilization buffer (*Reagent B*) then optimizes the dye fluorescence and dissolves cell aggregates by increasing the pH of the cell mixture. When the cell suspension was pretreated, all existing cells were counted. However, when the cell suspension is directly stained without pretreatment, nuclei from nonviable cells (i.e., with

disrupted plasma membrane) can be counted, and the cell viability proportion can be calculated.
In Paper I, cell counting and/or cell viability were determined in suspensions of detached cells, which were shaken from the surface of retrieved implants, and in exudates obtained by the lavage of peri-implant tissues and sham-wounded tissues.

### 3.4.3. Cytotoxicity

A widely used laboratory technique to assess cytotoxicity in biological samples is quantifying titers of lactate dehydrogenase (LDH), an enzyme that catalyzes the final conversion of pyruvate to lactate in glycolysis. LDH resides in the cytoplasm of all cells and is rapidly released extracellularly when the plasma membrane is disrupted in apoptosis, necrosis, and other forms of cellular damage.
Enzymatic photometry was performed with LDH-mediated lactate-pyruvic acid conversion in exudate samples collected by the lavage of peri-implant soft tissues or sham tissues (C-laboratory, Sahlgrenska University Hospital, Gothenburg), and the concentration of LDH (and therefore cytotoxicity) was measured in Paper I.

### 3.4.4. Cytocentrifugation (Cytospin)

Cytocentrifugation allows the isolation and deposition of a monolayer of cells from a dilute cell suspension onto a microscopic slide through centrifugal force. This technique offers the opportunity to microscopically examine cellular populations from a suspension after fixation and staining; however, the cellular concentration and centrifugal force must be optimized to prevent morphological artifacts.
In Paper I, cytospin was used for the microscopic examination of cells in exudate samples collected in implanted soft tissues and sham soft tissues upon staining with May-Grünwald-Giemsa. The proportions of polymorphonuclear cells (neutrophils) and mononuclear cells were calculated.

## 3.5. IMMUNOLOGICAL METHODS

### 3.5.1. Immunohistochemistry

Immunohistochemistry was instrumental in the present thesis for the *in situ* detection of proteins in tissue and for determining their spatial localization in a quantitative fashion. The identification of proteins in tissues at the microscopic level herein relied on the utilization of an antigen (i.e., protein)-specific antibody labeled with an enzyme that generates a colorimetric reaction, although labeling can also be achieved via a fluorescent marker. Antigen detection is, in fact, the final step in a sequence of essential procedures. Once the formalin-fixed paraffin-embedded tissue section is deparaffinized, the antigen that was crosslinked by the

fixative agent is unmasked through heat. Then, nonspecific binding sites are blocked using matched-species serum (goat serum), and endogenous peroxidase is inactivated. Immunolabeling is then performed through antibody-conjugated enzymes (horseradish peroxidase, HRP) that produce a chromogenic signal under the following prerequisites: completion of specific antibody-antigen binding and incubation with a chromogenic substrate (DAB).
Immunohistochemistry was used in Paper I, Paper II, and Paper III for the detection and quantification of cells expressing the proteins listed in **Table 3**.

***Table 3.*** *Panels of proteins targeted in Paper I, Paper II, and Paper III and related biological processes.*

| *Papers* | *Targeted protein* | *Related biological processes* |
|---|---|---|
| ***I*** | **iNOS,** | Macrophages (M1 subtype) |
| | **CD68** | Monocytes/Macrophages |
| | **MRC1** | Macrophages (M2 subtype) |
| | **ARG1** | Macrophages (M2 subtype) |
| ***II*** | **CD68** | Monocytes/Macrophages (mononuclear) |
| | | Osteoclasts (multinuclear) |
| ***III*** | **iNOS,** | Macrophages (M1 subtype) |
| | **CD68** | Monocytes/Macrophages (mononuclear) |
| | | Osteoclasts (multinuclear) |
| | **MRC1** | Macrophages (M2 subtype) |
| | **PIEZO1** | Mechanosensation/Ion channel |

**iNOS**: Inducible nitric oxide synthase; **MRC1**: Macrophage mannose receptor C type-1; **CD68**: Cluster of differentiation 68; **ARG1**: Arginase 1; **PIEZO1**: Piezo type mechanosensitive ion channel component 1.

### 3.5.2. ELISA

Enzyme-linked immunosorbent assay (ELISA) is a common analytical method used to quantify a variety of soluble substances, including proteins. In most ELISAs, the target antigen (i.e., protein) binds to an antibody immobilized on the microplate well surface (or other solid phase surfaces) as well as to an enzyme-labeled antibody, thus creating a 'sandwich complex' of well-antibody-antigen-antibody-enzyme. After the enzyme substrate is added, the amount of the resultant product, quantified by spectrophotometry, is proportional to the amount of the target protein in the sample.
After gene expression analysis, ELISA was used in Paper I to quantify the concentration of FGF2, VEGF, and iNOS in exudates from implanted soft tissue and sham soft tissue.

## 3.6. ELECTRON MICROSCOPY, SPECTROSCOPY, & X-RAY TECHNIQUES

### 3.6.1. Scanning electron microscopy

Scanning electron microscopy (SEM) enables surface imaging at high spatial resolution and high depth of field by applying a finely focused electron beam across a sample surface. The interplay between the emitted electrons and the atoms on the sample surface yields a range of signals. Among these, collected secondary electrons (SEs) and backscattered electrons (BSEs) provide information on the surface morphology and elemental composition.

***Secondary electron imaging*** − SEs are weakly bound electrons of the inner shell of the atoms on a sample surface (within a few nanometers) and are ejected due to the inelastic scattering interaction with the incident electron beam. In SE-SEM, the contrast generated by the difference in intensity between two neighboring regions results in 3D-like images with a high depth of field, which is valuable for the examination of surface topography.
In Paper I and Paper II, SE-SEM was used to visualize the implant surface before and after *in vivo* insertion. In Paper III, SE-SEM was used to image the osteocyte lacuno-canalicular network after resin-cast etching. In both settings, the conductivity of the sample surfaces was improved by coating with a conductive film to prevent static charge accumulation.

***Backscattered electron imaging*** − BSEs are high-energy electrons of an incident beam that are elastically scattered 'back' from the sample due to an interaction with the sample atom nuclei (at increased depth in comparison to SEs). Because the number of generated BSEs increases with the atomic number ($Z$), the contrast in BSE-SEM imaging can provide compositional information.
Through this 'compositional contrast', BSE-SEM was used to examine polished surfaces of hemi-sectioned Mg implants in Paper I and Paper II or bone in Paper II and Paper III. Areas composed of heavier elements, which appeared brighter (*bulk Mg* – Papers I and II; *bone matrix* – Papers II and III), were distinguished from those with lighter elements, which appeared darker (*degradation layer* – Papers I and II; *osteocyte lacunae* – Papers II and III). For BSE-SEM, surface conductivity enhancement with a conductive film coating was implemented prior to image acquisition.

### 3.6.2. Energy dispersive X-ray spectroscopy

In addition to generating electron signals, the interaction between a sufficiently energetic electron beam and a sample can also result in X-rays. Due to atom ionization in the sample by the incident electron beam, the ejection of an inner shell electron creates a core hole. This vacancy is then filled by an electron from

the higher energy shell, yielding an X-ray with an energy characteristic of the corresponding element in the periodic table. Therefore, energy dispersive X-ray spectroscopy (EDX) is used for elemental composition studies, although the spatial resolution might be hindered by an increase in the interaction volume.
EDX was used to investigate the elemental composition of the degradation layer at the surface of Mg-based implants in Paper I and Paper II, of bone interfacing with the implants in Paper II, and of the tissues around voids in Paper III.

### 3.6.3. Micro-Raman spectroscopy

The Raman effect is generated by the inelastic scattering of photons by molecules within a sample. In most instances, when an incident photon (i.e., from a laser) interacts with a sample, an emitted photon is elastically scattered at the same wavelength. However, the *incident photons–sample* interaction occasionally (~1 x $10^7$ photons) causes photons to scatter at a lower frequency than that of incident photons. This inelastic scattering is generated by a partial energy transfer from the incident photon to the sample molecules that become excited in vibrational states. Given that vibrational states are molecule specific, spectroscopy-based determination of the energy shift by inelastically scattered photons (presented as frequency/wavelength in $cm^{-1}$) yields information on the molecular composition of the sample.
In Paper II, micro-Raman spectroscopy was used to study the composition of the bone matrix at the interface with implants in comparison with native bone, thus expanding the elemental information obtained beforehand from energy-dispersive spectroscopy. Using point analysis, Raman metrics comprised mineral crystallinity [the reciprocal of the full width at half-maximum (1/FWHM) of the $\nu_1$ $PO4^{3-}$ peak], carbonate-to-phosphate ratio ($\nu_1$ $CO_3^{2-}/\nu_2$ $PO4^{3-}$), and the relative amounts of phenylalanine (Phe/$\nu_1$ $PO4^{3-}$). In Paper III, micro-Raman spectroscopy was implemented to collect spectra at each pixel of rectangular areas (hyperspectral maps) and from line scans. Through this method, the compositional fingerprint of tissues around peri-implant voids can be compared to that of native bone and synthetic hydroxyapatite.

### 3.6.4. X-ray microcomputed tomography

X-ray microcomputed tomography (micro-CT) is an X-ray absorption-based imaging technique through which the 3D internal architecture of a sample can be nondestructively visualized and analyzed at a micrometer-level spatial resolution. 2D radiographic projections, resulting from the attenuation of X-rays transmitted through the sample, are first produced at different rotation steps of the micro-CT stage (typically over 180°-360°). Through the subsequent mathematical reconstruction of these projections, a 3D representation of the geometry and microarchitecture of the specimen is generated. Micro-CT was used to study the bone microstructure of tibia metaphyses in Paper II and to visualize mineralized tissues around peri-implant voids in Paper III.

## 3.7. OTHER ANALYTICAL TECHNIQUES

### 3.7.1. Inductively coupled plasma optical emission spectroscopy

Inductively coupled plasma optical emission spectroscopy (ICP–OES) uses the energy from high-temperature plasma to excite atoms and ions in a sample (typically a solution), therefore moving electrons to higher energy levels. Hence, photons with a wavelength characteristic of the element are generated when the electrons return to the ground state. When the intensity of photons detected in a sample is spectrophotometrically determined, compositional information is obtained, and a specific element can be quantified.
In Paper I, ICP–OES was critical in monitoring the concentration of $Mg^{2+}$ in exudate from implanted soft tissue and sham soft tissue.

### 3.7.2. Small-angle and wide-angle X-ray scattering

In small- and wide-angle X-ray scattering (SAXS and WAXS, respectively), the sample is illuminated with defined-energy X-rays, resulting in elastic scattering. The scattering intensity, which is determined by patterns generated by constructively interfering scattering waves, is then recorded in an appropriate area detector and plotted as a function of the $2\theta$ angle (between incident and scattered X-ray beams). This angle can be small (SAXS, less than 10°) or wide (WAXS, larger than 10°) and provides different information on the ultrastructure of the studied material at a length scale ranging from angstroms to microns. SAXS might provide information on the size, shape, and arrangement of particles in a system, while WAXS provides information on the internal structure of a crystalline material.
In Paper II, synchrotron SAXS and WAXS were used to study trabecular bone ultrastructure in tibia metaphyses through the following metrics: thickness of the crystal platelet (SAXS), crystallite size and lattice spacing (WAXS).

### 3.7.3. *In vitro* immersion test

The most widely used technique for studying the degradation behavior of Mg metals consists of immersing the sample to test in a corrosive solution. Different immersion media can be used, and simulated body fluid (SBF) or cell culture media, such as Dulbecco's modified Eagle medium (DMEM), are among the most popular. In addition to the inorganic ions that constitute SBF, cell culture media exhibit several advantages, as the media involves small molecules of organic nature, such as amino acids. To further mimic *in vivo* conditions, proteins, such as fetal bovine serum, are increasingly used to complement cell culture media for immersion tests; when these proteins are used, an additional step to renew used media in a dynamic or semistatic fashion is often performed in tandem. Collecting the media provides an opportunity to monitor numerous metrics of degradation, including the following: pH, osmolality (concentration of all particles dissolved in

the medium), hydrogen release, etc. In addition, the retrieved implant from the media allows the calculation of its weight loss imputable to degradation. To achieve this, the degradation layer is typically removed (using chromic acid) to prevent the difference in weight before and after the implants are immersed from being over- or underestimated.
In the present study, immersion tests were performed to characterize the *in vitro* degradation behavior of pure Mg (Paper I, Paper II) and alloyed Mg (Paper II).

## 3.8. STATISTICS

Comparisons between all independent groups, i.e., comparisons between implants, were tested using nonparametric tests: Kruskal–Wallis and Mann–Whitney tests for multiple-group and two-group comparisons, respectively. All paired comparisons were tested through the nonparametric Wilcoxon signed ranked test except for the comparisons of detection intensities of elements between peri-void tissue *versus* native bone *versus* synthetic hydroxyapatite, which were tested using the parametric paired *t* test. Spearman correlation and linear regression analyses were performed to test statistical associations in SPSS (v.27; IBM Corporation). Differences for which $P<0.05$ were considered statistically significant. Differences for which $P<0.05$ were considered statistically significant. Hierarchical clustering, principal component, and correlation network analyses were performed in OriginPro (v.2023; OriginLab).

# 4. Results

## 4.1. PAPER I

*Promoter or quencher of inflammation?* – In the present study, the impact of the degradation of pure magnesium (Mg) implants on inflammation and subsequent repair and regeneration processes was investigated in soft tissues and compared to nondegradable titanium implants. To this end, the chronological and spatial patterns of cell distribution and activity at the tissue-implant interface were correlatively studied with the staged transformations of the Mg implant surface and $Mg^{2+}$ release over a 1–28 d observation period in rats. The main results are summarized in Figure 3.

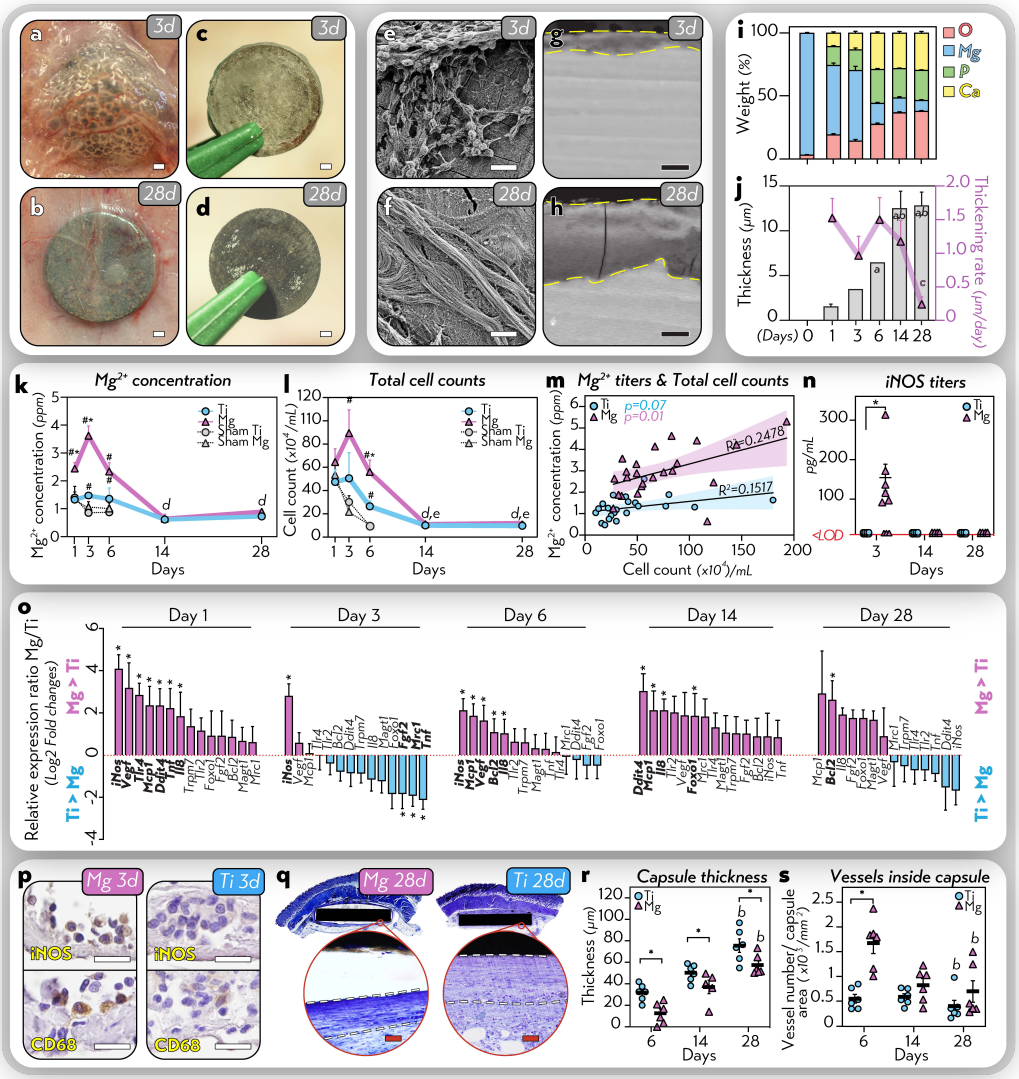

***Figure 3*: a-b,** Clinical photographs of the soft tissues surrounding Mg implants upon entry into the operated sites at 3 d and 28 d. **c-d,** Macroscopic observation of Mg implants immediately after collection from the 3 d and 28 d pockets. **e-f,** SE-SEM examination of the Mg implant surfaces showing the cellularity and the extracellular matrix. **g-h,** BSE-SEM examination of the Mg degradation layer (dashed lines) on implant cross-sections. **i,** Elemental composition of Mg implant surfaces at 1–28 d analyzed with EDX. **j,** Thickness of the Mg degradation layer at 1–28 d. **k,** $Mg^{2+}$ concentration in exudate samples. **l,** Counts of total cells in exudate samples. **m,** Linear regression of $Mg^{2+}$ concentration and total cell counts in exudate samples (data from 1 d, 3 d and 6 d pooled; 95% confidence intervals are shown). **n,** iNOS concentration quantified using ELISA in exudate samples. *<LOD:* measurement below the limit of detection. **o,** Differential gene expression between the Mg and Ti groups of cells attached to implant surfaces (log2 of the relative gene expression ratio). **p,** Immunohistochemistry to detect inflammatory cells positive for iNOS and CD68. **q,** Histology with toluidine blue of sections of Mg implants and surrounding soft tissues at 28 d highlighting peri-implant fibrous capsules (dashed lines in inserts). **r,** Thickness of the fibrous capsule around Mg and Ti implants. **s,** Density of blood vessels inside the peri-implant fibrous capsules (relative to capsule areas).
Data are mean ± s.e.m. n = 5-9/timepoint/group. * $P<0.05$ Mg *versus* Ti; # $P<0.05$ *versus* Sham Ti or Sham Mg; ***a:*** $P<0.05$ *versus* 1 d and 3 d; ***b:*** $P<0.05$ *versus* 6 d; ***c:*** $P<0.05$ *versus* 1 d, 3 d, 6 d, and 14 d.; ***d***: $P<0.05$ *versus* 1 d, 3 d, and 6 d in Mg; ***e***: $P<0.05$ *versus* 1 d, 3 d, and 6 d in Ti. Unpaired Mann–Whitney U test or paired Wilcoxon signed-rank test. Scale: **a,b** = 1 mm; **c,d** = 1 mm; **e,f** = 20 μm; **g,h** = 10 μm; **p** = 10 μm; **q** = 20 μm. Adapted with permission from [144] , Elsevier KeAi.

***The degradation of Mg implants initially elicited a profuse release of $Mg^{2+}$ and gradually enriched their surface in calcium and phosphorus*** – ICP–OES in exudate samples indicated that the interfacial concentration of $Mg^{2+}$ around Mg implants was substantially high from 1 d and 6 d and culminated at 3 d but markedly decreased thereafter. The slower degradation at the 14–28 d observation period was confirmed by the slower thickening of the degradation layer at the Mg implant surface, which was more concentrated in calcium and phosphorous, as shown by BSE-SEM and EDX.

***Inflammation but not cytotoxicity was amplified by the initial degradation of Mg implants*** – The initial (1–6 d) degradation of Mg implants elicited a vigorous chemotactic effect at the implant-tissue interface. This was reflected by the marked elevation of interfacial cell counts and mRNA levels of inflammatory cytokines (*Tnf*) and chemokines (*Il8, Mcp1*). In particular, the proinflammatory macrophage marker *iNos* consistently featured the highest expression among all considered genes for qPCR at the 1–6 d period, alongside elevated protein levels in exudates and soft tissues around Mg implants, as demonstrated by ELISA and immunohistochemistry, respectively. The gene ratio *iNos/Mrc1* (proinflammatory macrophage marker-to-prohealing macrophage marker) was clearly shifted toward

*iNos* over the 1–6 d period, indicating that the regulation of macrophage polarization favored the proinflammatory phenotype. In support of the relationship between Mg implant degradation and the intensification of the inflammatory response, $Mg^{2+}$ concentration exhibited a robust positive association with cell counts and with mRNA and protein levels of iNOS in the same exudate samples. However, neither viable cell fraction nor LDH titers were precluded by Mg implant degradation; thus, no cytotoxic effect was observed to accompany the amplification of inflammation in response to Mg implants.

***Inflammation in response to Mg implants was transient and enabled the onset of a thinner and more vascularized fibrous capsule*** − At 14–28 d, cell counts and inflammatory mRNA/protein markers (such as iNOS, TLR4, CD68) at the interface with Mg implants depicted a substantial attenuation, and correlated with the decreased per-implant release of $Mg^{2+}$. Concomitantly, soft tissues interfacing with the calcium- and phosphorus-enriched surface of Mg implants featured a thinner fibrous capsule with an increased number of blood vessels, as indicated by histomorphometry. This morphological evidence of an increased vascular supply in soft tissues associated with Mg implants was concomitant with the promotion of neoangiogenesis gene *Vegf* expression as early as 1 d in this group. The attenuation of fibrous encapsulation corresponded with the negative relationship between *Fgf*2 mRNA levels and $Mg^{2+}$ concentration at the interface with Mg implants.

***Mg implant degradation modulated the expression of markers of inflammation and tissue repair beyond the interfacial tissues*** − In sham sites (at a distance of ~2 cm from Mg implants), exudate samples intriguingly exhibited an initial, transient rise in the expression of several genes, such as *Il8*, *Mcp1*, *iNos*, and *Vegf*, with notable similarities to gene expression patterns at the interface with Mg implants. Atypical voids reminiscent of gas-generated cavities were also macroscopically and microscopically detected in sham soft tissues, without evidence of increased $Mg^{2+}$ concentration in their exudates. Together, these findings indicated that the amplified inflammation in sham sites might be plausibly linked to the gas released from Mg implants.

## 4.2. PAPER II

*Does immunomodulation by Mg implants, which was observed in soft tissues, also occur during the inflammation stage in bone? How is coupled bone healing altered?* – In this study, a rat osseointegration model was employed to investigate the 3 d- and 28 d-cellular response and assembly of bone reciprocally with surface alterations of Mg implants inherent in degradation. Implants fabricated from two different Mg-based materials, i.e., pure Mg and clinical-grade Mg alloy, were tested in comparison with nondegradable titanium analogs. The main results are summarized in Figure 4.

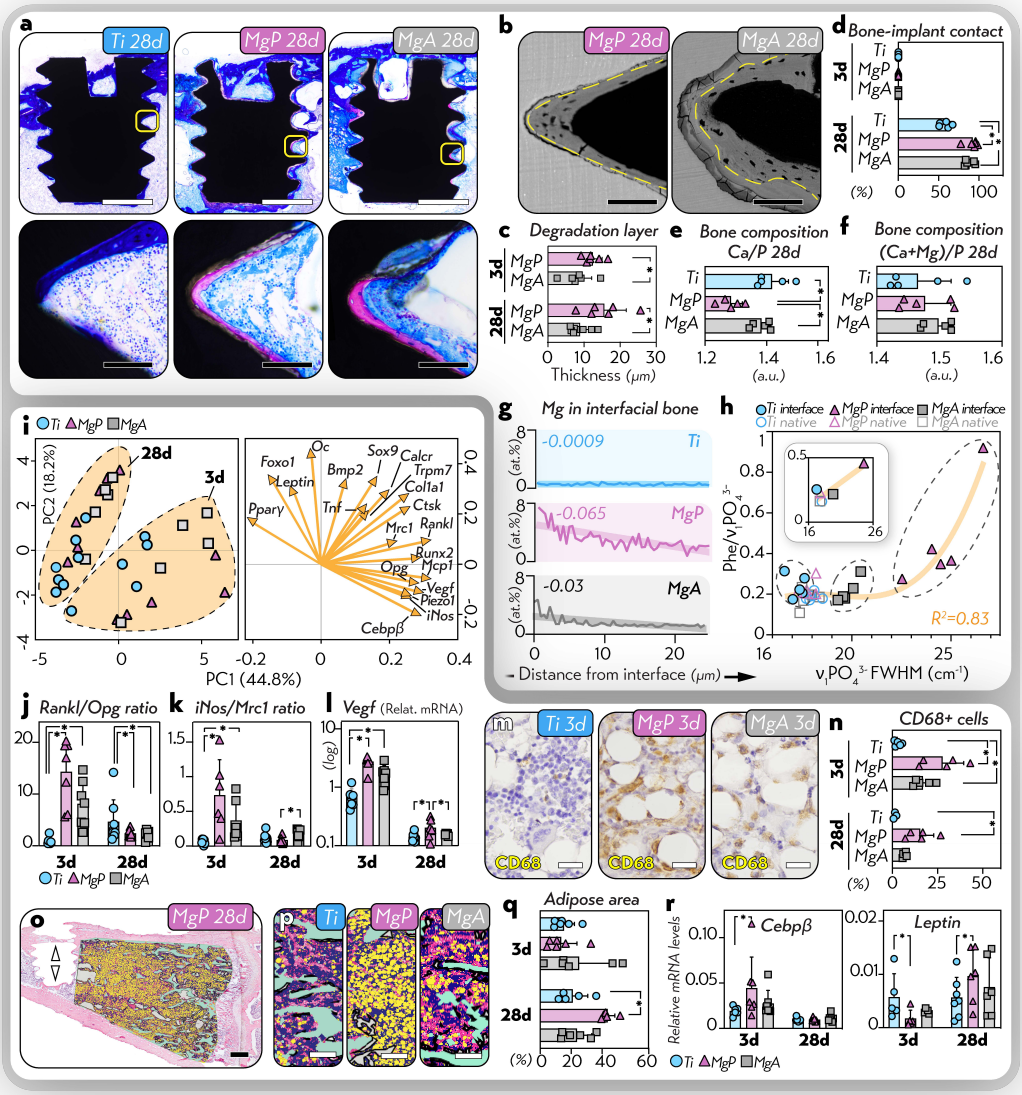

***Figure 4*: a,** Histology with toluidine blue at 28 d showing bone deposition at the surface of titanium (Ti), pure Mg (MgP), and alloyed Mg (MgA) implants. **b,** BSE-SEM observation of MgP and MgA implant cross-sections demonstrating the degradation layer interfacing with bone (interface highlighted by the dashed line). **c,** Thickness of the degradation layers atop MgP and MgA implants. **d,** Bone-implant contact in histology. **e-f,** Elemental composition of the interfacial bone determined with EDX line scans. Ca/P and (Ca+Mg)/P ratios averaged over the full bone thickness at the interface (atomic percentages). **g,** Averaged EDX spectra of bone 25 µm from the bone-implant interface showing Mg detection. **h,** Micro-Raman spectroscopy of the bone-implant interface at 28 d. Point measurements were performed at ~10 µm ('*interface*) from the bone-implant interface and in the native bone of the opposite cortex. The relationship between FWHM and Phe/$\nu_1PO_4^{3-}$ at the '*interface*' and '*native*' locations is shown with a third-order polynomial regression line (clusters of '*interface*' measurements in Ti, MgP and MgA are highlighted with dashed lines). **i,** Principal component analysis score plot (*left)* showing gene expression replicates in the peri-implant bone with 3 d and 28 d clusters and the corresponding loading plot (*right*) highlighting correlations between genes contributing to the between-replicates variance in the score plot. **j-k,** Ratio of relative mRNA levels by implant-adherent cells. **l,** Relative gene expression of *Vegf* by implant-adherent cells. **m,** Immunohistochemistry of the peri-implant bone showing CD68+ cells. **n,** Proportion of CD68+ cells in the peri-implant bone. **o-p,** Composition of the bone marrow surrounding the implants (implant site shown by the arrowhead) using semiautomated morphometry allowing the segmentation of fat (*yellow*), hematopoietic cellularity (*blue*), vessels and interstitium (*pink*), and bone (*green*) on histological sections stained with hematoxylin and eosin. **q,** Area proportion of the bone marrow adipose around the implants. **r,** Relative mRNA levels of markers of adipogenesis in the peri-implant bone.
Data are shown as the mean ± s.d. n = 5-8/timepoint/group. * $P<0.05$ Ti *versus* MgP *versus* MgA. Scale: **a:** *White* = 1 mm; *Black* = 50 µm; **b** = 50 µm; **m** = 20 µm; **o** = 1 mm; **p** = 100 µm.

***Pure Mg and alloyed Mg exhibited different degradation behaviors*** – BSE-SEM demonstrated that the *in vivo* thickness of the degradation layer was consistently higher at the surface of pure Mg implants than at the top of alloyed Mg implants inserted in bone. This finding, which indicated that pure Mg degrades faster than alloyed Mg, was partially confirmed by the semistatic *in vitro* immersion test; a notably alkaline pH was observed in the immersion media at 3 d, and a greater weight loss occurred over a 1–28 d period upon immersion of pure Mg implants.

***Pure Mg and alloyed Mg implants transiently intensified inflammation and activated neoangiogenesis*** – qPCR revealed that inflammation pathways were substantially activated at the interface with both Mg-based implants after 3 d. In comparison to titanium implants, pure and alloyed Mg implants upregulated the interfacial gene expression of the chemokine *Mcp1* and the proinflammatory macrophage marker *iNos* by more than 6-fold and 3-fold, respectively. At the interface between bone and pure and alloyed Mg implants, the gene ratio *iNos/Mrc1* (proinflammatory macrophage marker-to-prohealing macrophage

marker) was more than 10-fold and 5-fold higher, respectively, than at the bone–titanium interface. In parallel with the upregulation of inflammation-related genes, the neoangiogenesis marker *Vegf* also exhibited higher mRNA levels in response to pure and alloyed Mg implants at 3 d. Immunohistochemistry demonstrated elevated densities of CD68+ cells around both Mg-based implants at 3 d. At 28 d, most inflammation-related genes featured notably lower levels at the interface with both Mg-based implants, although the associated bone consistently featured elevated numbers of CD68+ cells, particularly around pure Mg implants.

***Bone formation and remodeling were promoted around both Mg-based implants, but pure Mg altered the composition of interfacial bone*** – qPCR demonstrated that gene markers of bone formation, such as *Oc* and *Col1a*, were highly upregulated at 28 d around pure and alloyed Mg implants. Concomitantly, the osteoclastogenesis genes *Ctsk* and *Calcr* also featured markedly elevated levels in response to both Mg-based implants. The potent changes in osteoclastic regulation were further illustrated by the *Rankl/Opg* gene ratio. At 3 d, this ratio was 17-fold and 8-fold higher at the interface with pure and alloyed Mg implants, respectively, than at the interface with titanium implants. However, at 28 d, the *Rankl/Opg* gene ratio shifted and was over 2-fold higher at the interface with titanium than at the interface with both Mg-based implants. This gene expression pattern, indicating the coupled accelerated activation of bone anabolic and catabolic pathways, was associated with a high deposition of bone at the surface of pure and alloyed Mg implants, as evidenced at 28 d by the bone-implant contact calculated on histological and BSE-SEM images. However, EDX and micro-Raman spectroscopy showed that bone interfacing with pure Mg was compositionally distinct from bone interfacing with alloyed Mg and titanium implants. This was revealed by the lower Ca/P ratio by EDX alongside the lower mineral crystallinity [(1/FWHM) of the $\nu_1\ PO_4^{3-}$ band] and the increased relative content in Phe (Phe/$\nu_1\ PO_4^{3-}$), all of which indicated 'younger' bone at the interface with pure Mg implants.

***Pure Mg implants increased adipose tissue in the neighboring bone marrow*** – Histology revealed that bone marrow in tibia metaphyses implanted with pure Mg implants unexpectedly contained more adipose tissue than in tibia with alloyed Mg or titanium implants at 28 d. The bone marrow neighboring pure Mg implants contained ~2-fold larger adipose fraction and ~2-fold more adipocytes compared to bone marrow associated with alloyed Mg and titanium implants. Moreover, the adipocyte size was larger in the bone marrow surrounding the pure Mg implant. This increased adiposity at 28 d was particularly noticeable in bone marrow very close to pure Mg implants where adipocytes were jointly localized with CD68+ cells at 3 d. qPCR further demonstrated the staged activation of proadipogenic pathways in bone neighboring pure Mg implants. This was pictured at 3 d by the gene upregulation of *Cebp*, which denotes the initiation of adipogenic differentiation, and at 28 d by the elevated mRNA level of *leptin*, a hormone specific to mature adipocytes. Despite the increased adiposity, micro-CT, SAXS and WAXS analyses did not show structural alterations in the trabecular bone in tibia metaphyses with pure Mg implants.

## 4.3. PAPER III

*Do the voids generated by gas release from Mg implants promote inflammation? Does mechanosensation play a role in the response to these voids?* – The intensified inflammation observed far from soft tissue (sham sites) in animals implanted with pure Mg implants in Paper I led to uncertainties regarding the contribution of gas to the inflammatory response to these implants. In Study 3 (paper III), the phenotypic regulation of cells near gas-generated voids was studied in the following tissue environments in rats implanted with pure Mg: soft tissue (1 d, 3 d, 6 d, and 28 d) and bone (3 d, 28 d). The main results are summarized in Figure 5.

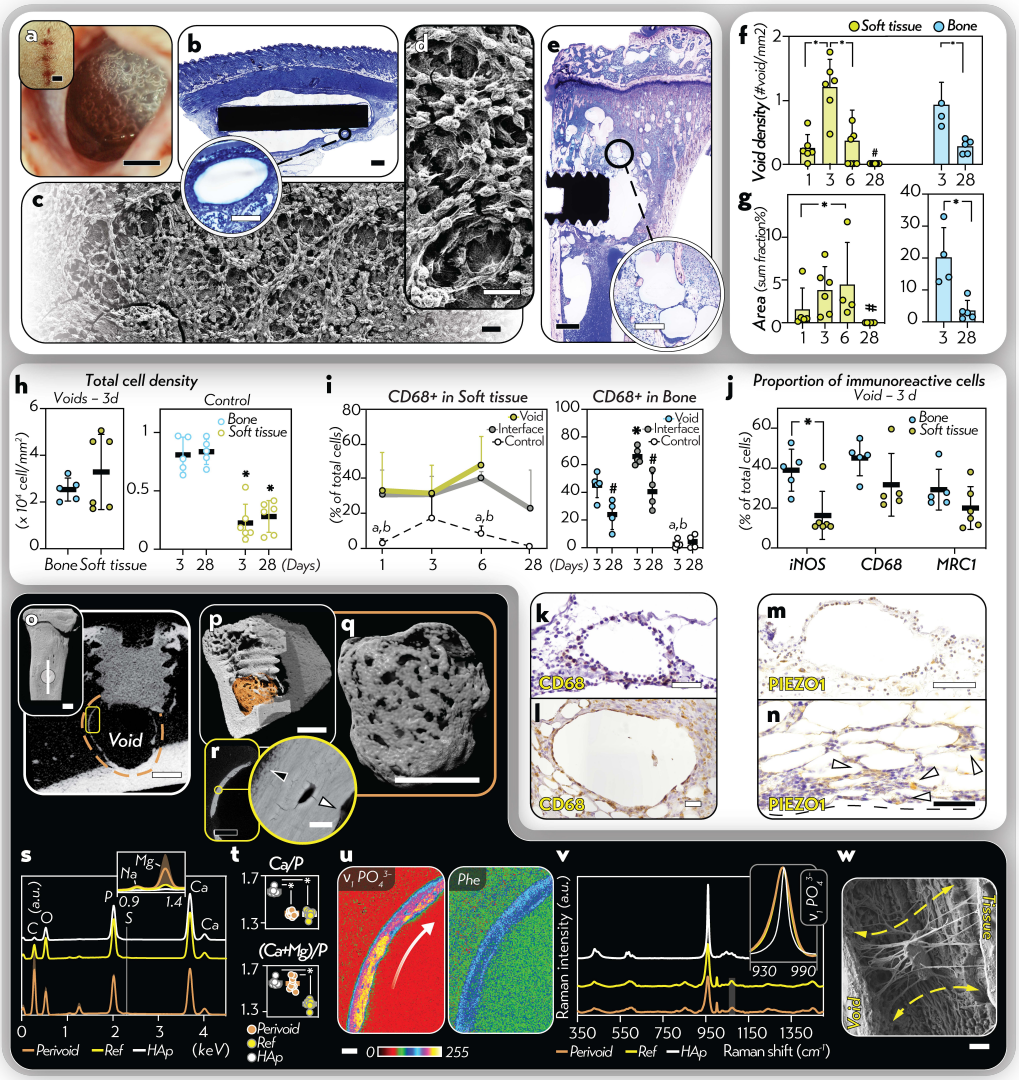

***Figure 5*: a,** Photographs showing subcutaneous pockets implanted with a pure Mg disc and re-entered at 3 d. Upon implant retrieval and lavage of the peri-implant tissues, several bubble-shaped features were visible in the thickness of the peri-implant fascia. **b,** Histology with toluidine blue enabled the microscopic examination of the gas voids, demonstrating the presence of soft tissues encircling the voids. **c-d,** SE-SEM examination of the surface of implants in soft tissues, depicting the organization of cells and extracellular matrix, which was comparable to the microscopic features of gas voids in histology. **e,** Histology with basic fuchsin and methylene blue of bone implanted with a pure Mg screw, demonstrating the presence of numerous peri-implant voids. **f-g,** Density of voids and void area fraction in soft tissue and bone (fraction of the sum void area from the total area of the subcutaneous fascia or bone marrow). **h,** Density of total cells within 20 µm from the voids – *Void*, and at a distance from the interface – *Control* (circular region with an area equal to the average area of detected voids in soft tissue or bone). **i,** Proportion of cells immunoreactive to CD68 among total cells detected in the regions of interest in soft tissue and bone analyzed by immunohistochemistry. **j,** Comparison of the peri-void immunoreactivity to iNOS, CD68, and MRC1 between soft tissue and bone at 3 d. **k-l,** Immunohistochemistry showing voids in soft tissue (**k**) and bone (**l**) surrounded by CD68+ cells. **m-n,** Immunohistochemistry showing PIEZO1 protein expression in cells around voids in soft tissue (**m**) and bone (**n**). **n,** shows a magnified area; broken line outlines the interface with the void; arrowheads show PIEZO1+ cells. **o-q,** Micro-CT of a pure Mg implant in the tibia featuring a mineralized matrix interposed between the implant apex and the opposite cortex. **r,** BSE-SEM revealed osteocyte-like lacunae embedded within the mineralized matrix surrounding the void. The outer surface (black arrowhead; *toward the bone marrow*) displayed ongoing mineralization that could not be observed on the inner surface (white arrowhead; *toward the void*). **s-t,** Elemental composition of the region highlighted in (**r**) was analyzed with EDX and compared to that of the native bone (opposite cortex) and the synthetic hydroxyapatite. **u,** Raman maps of the $\nu_1PO_4^{3-}$ peak (930-990 $cm^{-1}$ integral area) and Phe peak (990-1015 $cm^{-1}$ integral area). The arrow shows the implant direction. **v,** Spectra of the peri-void bone-like matrix, native bone, and synthetic hydroxyapatite corresponding to maps in (**u**). The inset shows the $\nu_1PO_4^{3-}$ peak. **w,** Resin-cast etching revealing an osteocyte in the mineralized matrix around the void with a canalicular system displaying a preferential directionality *void-bone marrow*.
Data are shown as the mean ± s.d. n = 5-6/timepoint/group. * $P<0.05$ Soft tissue *versus* Bone (Void or Control) or Void *versus* Interface. **#**, $P<0.05$ Day 3 *versus* Day 28 in the same group. **a**, $P<0.05$ Void *versus* Control. **b**, $P<0.05$ Interface *versus* Control Mann–Whitney U test unpaired comparisons. Friedman's two-way analysis of variance by rank for paired comparisons of Void *versus* Interface *versus* Control. Scale: **a,b:** *Black* = 1 mm; *White* = 100 µm; **c,d** = 20 µm; **e:** *Black* = 1 mm; *White* = 200 µm; **k-l-m** = 50 µm; **n** = 20 µm; **o-q** = 1 mm; **r:** *Black* = 200 µm; *White* = 20 µm; **u** = 50 µm; **w** = 5 µm.

***The morphology of gas voids changed over time*** – In soft tissue and in bone, gas voids were detected in high numbers over the initial days after implantation but were infrequently observed by 28 d. Gas voids in soft tissues, which typically exhibited an ellipsoidal shape, were surrounded by a considerable accumulation of

cells in contrast with the scattered cells populating the peripheral connective tissue. The area of these voids had an ~3-fold increase from 1 d to 6 d, but no voids were observed at 28 d. In bone, gas voids, which had a near-circular shape, decreased by ~6-fold in size between 3 d and 28 d. Bone gas voids were also outlined by elevated counts of cells at 28 d.

***Gas voids exacerbated the inflammation of nearby cells in soft tissue and in bone*** – Compared to cells within 20 μm from the interface between implants and soft tissue and the interface between implants and bone, cells within 20 μm from the voids populated tissues at a markedly higher density. This contrast in cellular density suggested that cells experienced a robust attractant effect by gas voids; this effect was even more pronounced when comparing tissues outlining the voids to those located away from the implant and from associated voids in both tissue environments. Immunohistochemistry further demonstrated that many cells near the voids (within 20 μm) exhibited an evident inflammatory phenotype; their immunoreactivity to macrophage markers CD68, iNOS, and MRC1 was often as elevated as at the soft tissue–implant interface or the bone–implant interface, particularly during the initial observation period (1–6 d) and at a lower level afterward (by 28 d). The tissue environment influences the inflammatory response. For instance, the proportion of iNOS+ cells close to the voids at 3 d was clearly higher in bone than in soft tissue.

***Mechanotransduction pathways were activated in tissues surrounding the voids*** – Close examinations of cells near the voids in soft tissue and bone consistently revealed that the cells acquired a spindle-like shape, possibly due to mechanical cues exerted by the voids on the surrounding cells. Immunohistochemistry confirmed that mechanosensitive protein PIEZO1 was markedly expressed by cells around the voids in soft tissue and in bone as compared to control areas. In addition, higher proportions of PIEZO1+ cells were found at the soft tissue–implant and bone–implant interfaces compared to that around voids in soft tissue and bone, and compared to control areas. No differences were found in PIEZO1+ cell proportions between soft tissue and bone at 3 d.

***Bone was occasionally deposited around the voids*** – In 2 of the 8 tibiae implanted with pure Mg screws at 28 d, a mineralized matrix surrounded the voids, interposed between the implants and the opposing cortex, as revealed by micro-CT. Histology indicated that these mineralized entities exhibited a morphological resemblance to bone, as suggested by the presence of osteocyte lacunae and vascular canals enclosed in a lamellar matrix. Ongoing mineralization at the outer surface of this matrix and toward the implant was demonstrated by histology and BE-SEM. In comparison to native bone, this matrix had a lower mineral content but a higher organic content (Phe); this composition indicated a 'younger' stage of mineralization, as shown by micro-Raman spectroscopy. EDX elemental mapping further suggested that this matrix was enriched in Mg, particularly in areas closer to the implant. A closer examination of the osteocytes revealed that they were aligned in parallel to the voids. Numerous canaliculi of these osteocytes appeared to closely contact the voids as well as the surrounding bone marrow. Thus, a

preferential *void–bone marrow* directionality of the osteocyte canaliculi was noticeable in clear contrast with the lacuno-canalicular network of osteocytes in the native bone.

# 5. Discussion

## 5.1. THE EARLY PHASE AFTER MAGNESIUM IMPLANTATION: IMMUNOMODULATION IN SOFT TISSUE & BONE

The initial host response to an implant, i.e., the proinflammatory phase in the microvasculature, is considered to be decisive in its integration into the accommodating tissues [145, 146]. Regardless of the nature of the tissue, this proinflammatory response was markedly amplified by the degradation of Mg implants in comparison to that of nondegradable titanium implants (Paper I, Paper II). This observation goes against the hypothesis of an anti-inflammatory effect of Mg metallic implants, at the early phase of healing. In fact, during the initial reaction to Mg implants, the modulation of two critical cellular behaviors stood out as central: leukocyte recruitment and the proinflammatory polarization of macrophages.

Chemotaxis is a pivotal biological process in the initial response whereby signaling molecules are released into injured tissues to mobilize leukocytes [147, 148]. Mg implants strongly increased interfacial cellularity (Paper I) and elevated mRNA levels of numerous chemotactic markers, including *Tnf*, *Mcp*, and *Il8* (Paper I and Paper II). Among the leukocytes attracted to tissues interfacing with Mg implants, high proportions of neutrophils and proinflammatory macrophages were present (Paper I and Paper II), and both cell types are known to be vital for wound debridement and for guiding tissue repair and regeneration[149-151]. An important finding was that the $Mg^{2+}$ concentration in the exudate was strongly linked to the number of recruited cells and to the gene and protein expression levels of the marker of proinflammatory macrophage iNOS at the interface with Mg implants. Therefore, it is reasonable to assume that the amplified chemotaxis and the proinflammatory polarization of macrophages stem from the initial burst release of $Mg^{2+}$ from these implants. Exogenous metal ions are capable of potentiating chemotaxis. For example, $Cu^{2+}$ released from the degradation of copper implants *in vivo* amplifies cellular recruitment to the implant surface [152, 153]. Supplementation of cells with $Ca^{2+}$ *in vitro* is also known to increase chemotaxis [154] through the promotion of cell mobility via the breakdown of intercellular junction proteins [155]. In addition, recent *in vivo* evidence suggests that $Mg^{2+}$ released from hydrogels encourages a proinflammatory environment through CD68+ macrophage recruitment [111, 156]. However, the possibility should not be excluded that other degradation products may also contribute to the cellular attraction and to the proinflammatory behavior of recruited cells in tissue implanted with Mg metallic biomaterials. Among these, gas cavities in soft tissues and in bone (Paper III) were capable of eliciting *in situ* attraction of a large population of cells that featured elevated immunoreactivity to iNOS and CD68. Other byproducts, such as reductive species, including reactive oxygen and nitrogen species, may also play a role in fostering such a proinflammatory environment [157] in response to Mg implants [158] via yet-to-be-illuminated ways.

Ion release has been associated with increased cytotoxicity underlying severe tissue damage in patients with cobalt-chromium implants [159]. Recent evidence also suggests that the initial Mg degradation may aggravate injury-induced hypoxic conditions through local oxygen reduction reactions at the Mg implant surface [160, 161]. Therefore, it may be assumed that such microenvironment conditions are unhospitable for living cells, especially given the magnitude of the initial proinflammatory response to Mg implants. Our results (Paper I) refute this hypothesis and show that no cytotoxicity is elicited by the degradation of Mg implants. The present finding that the degradation of Mg implants does not hamper cellular viability is of paramount importance in supporting the concept of biocompatibility of metallic Mg implants. Two rationales may be advanced to explain why these implants did not detain the deleterious effects documented for cobalt-chromium implants. One explanation is that neutrophils, monocytes, and macrophages, which represent a large proportion of cells interfacing with Mg implants (Paper I, Paper II), are phylogenetically equipped to cope with the initial challenging conditions postinjury [162]. For instance, macrophages of the proinflammatory phenotype (M1) are able to switch toward anaerobic energy production [163]. The second and more important factor in determining the absence of a cytotoxic outcome is the transient nature of the initial proinflammatory responses. In fact, the early responses to Mg implants were characterized by marked switches from proinflammatory to proregenerative regulation. The most evident representation of this shift was the sequential change in mRNA and protein signaling from the priming of M1 macrophages to M2 macrophages, irrespective of the type of tissues interfacing with Mg implants (Paper I and Paper II). Importantly, the present findings also indicate that this resolution of the initial, exaggerated inflammatory response occurred in soft tissue (Paper I) and in bone (Paper II) in tandem with a slower degradation of Mg implants. Although synergy between exogenous $Mg^{2+}$ and the phenotypic regulation of macrophages has been linked *in vitro* to the $Mg^{2+}$ channels TRPM7 [164] and MAGT1 [165], no such associations were found on the gene expression level in soft tissue (*Trpm7*, *Magt1*; Paper I) or in bone (*Trpm7*, *Paper* II), presumably due to functional intersections *in vivo* with other ion channels (e.g., TRPM6 [91]).

## 5.2. REPAIR/REGENERATION OF SOFT TISSUE & BONE IN RESPONSE TO MAGNESIUM IMPLANTS AND THEIR IMMUNE PATHWAYS

The repair and regeneration of wounded tissues are intricate, multifaceted processes that depend heavily on the nature and magnitude of the preceding inflammatory response [166]. The resolution of the proinflammatory response after an injury is key to enabling 'proper' tissue repair or tissue regeneration. However, if this initial inflammation becomes dysregulated, or *chronic*, upon the introduction of an implant into tissues, an aberrant fibrotic reaction occurs [167]. To better comprehend how immune pathways can drive different aspects of tissue repair, let us compare two restorative scenarios and their linked inflammatory

programming in response to the implantation of two different biomaterials: titanium and copper.

Metallic copper implants, which degrade and release $Cu^{2+}$ upon contact with tissues, are cytotoxic [153]. They elicit a strong proinflammatory response [152], characterized by robust neutrophil recruitment [153, 168] in conjunction with high release of IL1α [152] and IL6 cytokines [168], which do not subside with time [169]. In contrast, nondegradable titanium implants [170], as we observed in Paper I, are noncytotoxic [153, 171] and induce a mild, transient proinflammatory response [152, 168] that quickly dissipates [172] (within the first two days after implantation in soft tissues). These divergent inflammatory responses to the biomaterials result in contrasting regenerative outcomes. In soft tissues, the dysregulated inflammatory reaction to copper implants leads to excessive fibrotic encapsulation compared to the response to titanium [169]. In bone, titanium implants successfully integrate into bone [173] whereas the uncontrolled inflammation associated with copper implants hampers osseointegration and leads to peri-implant fibrosis [174].

So, where do Mg implants stand in the spectrum of restorative scenarios and their inflammatory programming? – A hint to answering this question may reside in the dynamics of macrophage polarization.

The activation of proinflammatory macrophages via interactions with biomaterials is a strategy has been shown to be efficient in enhancing neoangiogenesis [175], mainly through the enhanced production of pro-angiogenic factors by these cells such as vascular endothelial growth factor (VEGF) [175]. Key in initiating and steering vessel sprouting during inflammation [176], VEGF was consistently expressed at elevated levels in soft tissue (Paper I) and in bone (Paper II) associated with Mg implants, corroborating a previously reported improvement in the vascular supply of tissues interfacing with Mg implants *versus* titanium implants [123].

Moreover, the conversion of proinflammatory macrophages to the prohealing phenotype is considered critical for the attenuation of fibrosis during tissue repair [149]. As documented regarding other biomaterials [177], the sequence of macrophage activation from the proinflammatory to the prohealing phenotype may underlie the observed morphological (i.e., thinner fibrous capsule) and molecular (i.e., increased expression of the antifibrotic gene Forkhead Box O1, *Foxo1*) evidence of an attenuation of fibrous encapsulation in the response of soft tissue to Mg implants *versus* titanium implants (Paper I).

In bone, our findings also indicate that a tight association may exist between this phenotypic transition of macrophages and a pronounced shift in the regulation of the receptor activator of nuclear factor κB ligand/osteoprotegerin (RANKL/OPG) system (Paper II). In sequence, Mg implants (both pure and alloyed) first markedly increased gene expression of *Rankl*, a key marker of osteoclastogenesis onset [178], before notably causing increased mRNA levels of the osteoclastogenic inhibitor *Opg* [178]. RANKL plays a pivotal role in the communication between proinflammatory macrophages and osteoclasts [179] through NF-κB signaling [180]. An initial, transient activation of osteoclasts by implants functionalized with lipopolysaccharide [181], which is also known to elicit the proinflammatory polarization of macrophages [182], notably enhances osteogenesis at the implant interface [181]. The ability of Mg implants to foster bone deposition in comparison

to titanium implants, as shown by the elevated bone–implant contact and the upregulation of osteogenesis-related genes in Paper II, is well-established [123, 183, 184]. Importantly, the present findings show that this osteogenic effect by Mg implants is preceded by a strong, transient activation of osteoclastogenesis that occurs in synchrony with macrophage polarization. Our results, therefore, contradict the common perception, based on *in vitro* studies [185, 186], that Mg implants inhibit osteoclastogenesis [77, 187].

Beyond the nuanced reparative outcome between Mg and titanium implants delineated above, subtle variations in immune reactions in response to pure *versus* alloyed Mg implants in bone may also lead to unexpected reparative scenarios. Indeed, the faster degradation of pure Mg implants, but not of alloyed Mg implants, was associated with a previously unknown proadipogenic response in the bone marrow and a compositional alteration of the interfacial bone (Paper II), are major findings.

On the one hand, pure Mg implants activated mRNA pathways related to inflammation and osteoclastogenesis at a higher magnitude than that in response to alloyed Mg implants. It was therefore not surprising that at 3 d postimplantation, the bone marrow adjacent to pure Mg implants and even at remote distances from them was heavily infiltrated by proinflammatory macrophages expressing CD68. However, a surprising observation was that elevated proportions of these cells persisted in the bone marrow adjacent to pure Mg implants at 28 d and indicated the presence of aberrant, low-grade inflammation. Various pathophysiological processes may sustain a chronic state of inflammation in the bone marrow and alter the gene regulatory machinery to direct undifferentiated mesenchymal stem cells toward an adipogenic fate [188]. For example, the persistence of infiltrating CD68+ macrophages is a signature feature of adipose tissue dysfunction [189] and a hallmark of adiposity in obesity and diabetes [190, 191]. Another example is aging, which is documented to elicit an upregulated gene expression of *Rankl* via the early adipogenic transcription factor CCAAT-enhancer binding protein-beta (CEBPβ), resulting in the coprogression of fatty marrow and bone deterioration [192]. Although both *Rankl* and *Cebpβ* were found at elevated gene expression levels in response to pure Mg implants, such a joint deterioration of bone and marrow adiposity was not observed in our work, as the trabecular bone associated with the expanded marrow adipose tissue did not feature structural alterations (Paper II).

On the other hand, the bone interfacing with pure Mg implants at 28 d postimplantation was compositionally distinct from that interfacing with alloyed Mg and titanium implants (Paper II). Although bone was deposited in large amounts at the interfaces of pure Mg implants, its altered elemental components (decreased Ca/P ratio and increased detection of Mg) and lower mineral crystallinity (decreased 1/FWHM) may seem connected to the prevalent belief regarding the inhibition of apatite mineralization [193, 194]. For instance, this hypothesis was proposed to explain why the release of $Mg^{2+}$ from hydrogels in rat bones compromised the mineral density of the newly formed bone if prolonged beyond the initial postimplantation week (but not within this time window) [111]. Our results (Paper II) show that the organic fraction in bone interfacing with pure

Mg implants was high (i.e., elevated Phe/$\nu_1$ $PO_4^{3-}$), meaning that this interfacial bone was in a 'less aged' state [195]. This does not agree with the hypothesis regarding inhibition of apatite mineralisation by Mg implants. In addition, keeping in mind the osteoclastic activation in response to pure Mg implants, the hypothesis that the 'less aged' bone is due to increased bone turnover adjacent to these implants cannot be excluded. Whether such compositional alteration may alter the biomechanical anchorage of pure Mg implants also demands further scrutiny.

## 5.3. GAS BUBBLES AROUND MAGNESIUM IMPLANTS: INFLAMMATION AND TISSUE REPAIR LINKED TO MECHANOSENSATION?

Since the earliest utilization of Mg as biodegradable metallic implants, a feature unique to this biomaterial remained unaltered, even with the most recent sophistication in its tailoring: to generate gas bubbles in the surrounding tissues. However, the understanding of the biological impact of these voids has remained enigmatic and controversial. An intriguing finding in Paper I was the amplified inflammation in soft tissue (sham sites) at ~2 cm distance from Mg implants with features of cavities resembling gas voids. Paper III validates the impact of gas voids on inflammation and unveils a previously unrecognized effect: mechanosensation. As highlighted above in the Discussion, the contribution of gas voids in recruiting cells to the implantation site is undeniable. The finding that leukocyte densities around these cavities in soft tissue and bone (Paper III) were on par with cell densities in tissues interfacing with Mg implants indicates their strong attractant potency. Beyond the chemotactic outcome of Mg implants demonstrated in Paper I, the question that naturally arises is why these gas cavities attract cells locally. A postulate would be that the gaseous content may elicit cellular attraction. By quickly diffusing into tissues and across cell membranes [133], hydrogen would be a plausible candidate for eliciting paracrine signaling [134]. Small molecules that diffuse very rapidly into tissues can attract cells to the wound [196] even faster than soluble chemokines that need to travel through wound fluids [197]. However, given that hydrogen has been suggested to be present in small concentrations inside the gaseous pockets [139, 140], and that therapeutic hydrogen administration can alleviate chemotaxis [198], this hypothesis is unlikely. Instead, a more compelling assumption is that the mechanical cues may have a role in the cellular attraction. The stretched spindle morphology of the cells that surround them in soft tissue and bone (Paper III) indicated a pressure exerted by the voids. An increasing body of evidence suggests that mechanical stimuli can be as influential as chemical cues in driving cellular migration through key mechanotransduction pathways [199], in which the role of Piezo-type mechanosensitive ion channel component 1 (PIEZO1) appears to be diverse.

PIEZO1 operates as a mechanically sensitive ion channel. Stretch activation of PIEZO1 by mechanical cues allows the passage of cations (including $Ca^{2+}$ and $Mg^{2+}$) through the cellular membrane to engage downstream pathways [200]. PIEZO1

has widespread expression in cells across diverse tissues, including soft tissue and bone [201], and appears to link mechanosensation and inflammation [202, 203]. Upon pressure or shear stress stimuli, PIEZO1 activity facilitates the release of inflammatory cytokines and chemokines by monocytes and macrophages [204]. For instance, stenosis (i.e., narrowing) of the aortic valve inflicts high shear stress on circulating blood cells, resulting in a proinflammatory activation of monocytes and macrophages by activating PIEZO1 as their main mechanoreceptor. However, the replacement of the dysfunctional aortic valve with an implant reduces the shear stress and alleviates inflammation in a PIEZO1-dependent fashion [204]. Another example reflecting the critical role of PIEZO1 in mechanosensation and inflammation is the modulation of macrophage polarization in response to implanted biomaterials depending on the mechanical cues that they convey [205]. In comparison to soft biomaterials, stiff biomaterials implanted subcutaneously in mice increase cellular infiltration and encourage recruited macrophages to adopt a proinflammatory phenotype. However, in mice lacking PIEZO1, the soft tissue loses its ability to sense and respond to the implant stiffness. This translates into a decrease in leukocyte recruitment and proinflammatory macrophage polarization, regardless of the implant stiffness. Our findings (Paper III) demonstrate that cells in soft tissue and bone respond *in situ* to the gas void interface by early expression of PIEZO1 following implantation with Mg implants. Concomitantly, iNOS+ and CD68+ cells were present in high proportions and indicated proinflammatory macrophage polarization. It is therefore reasonable to assume that the mechanical stimulus caused by the gas voids primes recruited cells, notably macrophages, toward proinflammatory polarization. It is also interesting to note that this mutual activation of proinflammatory and mechanosensitive pathways around the gas voids was similarly found at the interface between Mg implants and both soft tissue and bone (Paper III) and confirms the elevated mRNA expression levels of *Piezo1* detected in response to these implants (Paper II). These results demonstrated a hitherto unidentified mechanosensitive component of the tissue response to Mg implants and their gas cavities.

This conclusion leads us to the question of how tissue repair proceeds around these gas voids. Our morphological findings that showed an accumulation of the extracellular matrix around soft tissue voids and of adipocytes around bone marrow voids over time are not surprising. Amplified inflammation is known to encourage such reparative outcomes in soft tissue [148] and in the bone marrow [188]. However, a surprising finding was that bone could also occasionally be deposited around gas voids in the bone marrow. How can bone grow in an inflammatory milieu under mechanical stimulation? Herein, drawing a parallel with scenarios where bone deposition is atypical could provide some clarity. Pathological new bone formation in conditions such as ankylosing spondylitis would be, indeed, of interest. Ankylosing spondylitis is an inflammatory disease in which pathological new bone formation elicits fusion (ankylosis) and chronic pain in ligaments and tendons of the spine [206]. Ligaments and tendons are, in general, subject to strong mechanical forces and are preferential sites of heterotopic ossification [207]. Interestingly, PIEZO1 activation by mechanical stimuli was recently revealed to play a dual role in the pathogenesis of ankylosing spondylitis in animals and in humans [206]. First, the activation of PIEZO1 upregulates the expression of multiple

proinflammatory cytokines, such as tumor necrosis factor (TNF) and interleukin 17 (IL-17), thereby sustaining an inflammatory state. Second, PIEZO1 activation, which is required in bone healing and remodeling [208, 209], prompts the differentiation of chondral- and osteal-lineage cells in the ligaments and tendons toward osteogenesis in synergy with the Wnt/β-catenin pathway [206]. Therefore, the combination of mechanical cues, PIEZO1 expression, and inflammation in ankylosing spondylitis is speculated to act as a feedforward loop that propels new bone growth outside the skeletal envelope [206]. This concept has been confirmed by recent evidence suggesting the combination of mechanical stimulation and inflammation as a common etiopathology of heterotopic ossification in different anatomical regions. [210]. In our work (Paper III), the atypical morphology of the lacuna-canalicular network of osteocytes in the bone around voids further supported an influence of mechanical stimulation. Speculatively, given that the combination of mechanical cues, PIEZO1 activation, and inflammation is found in the bone marrow surrounding gas voids, this triad might be an important factor behind the occasional bone formation around the voids in the bone marrow. Moreover, as it is also a channel that transports $Mg^{2+}$, whether the implant release of $Mg^{2+}$ might also alter the activity of PIEZO1 remains to be explored.

## 5.4. SOFT TISSUE *versus* BONE: INFLAMMATION AND TISSUE REPAIR/REGENERATION

In their responses to Mg implants, soft tissue and bone share evident similarities. Namely, these include: first, the onset of an amplified, transient inflammatory reaction (Paper I, Paper II, Paper III); second, the proper subsequent repair/regenerative processes (Paper I, Paper II); and third, the accumulation of cells (macrophages) and their local mechanosensitive responses around gas voids (Paper III). Other resemblances related to the behavior of Mg implants cannot be overlooked. Made of high purity Mg (>99.995%), implants in soft tissue and in bone feature comparable degradation kinetics: the degradation is initially active at the initial postimplantation week (1–6 d), before slowing until postimplantation week 4. Concomitantly, increasing accumulation of Ca and P over time was noticeable at the interfaces of pure Mg implants in soft tissue and bone. Widely documented *in vitro* [42] and *in vivo* [53, 211], this passive mineral deposition progressively confers protection to the surface of Mg implants against their corrosive tissue milieu. Evidence from *in vivo* experiments indicates that preventing Ca and P deposition using inhibitors, such as matrix GLA protein [212], accelerates Mg implant degradation. It is, therefore, reasonable to speculate that the onset of this mineral barrier, which is indispensable for slowing Mg degradation over time, plays a crucial role in guiding inflammation resolution and in facilitating tissue repair and regeneration, as we found in our work. Given the differences in the implant designs and that the monitoring of Mg degradation was based on the degradation layers and gas void morphometry in both soft tissue and bone, comparing the Mg degradation kinetics between the two tissue microenvironments appears inappropriate. Beyond mere two-dimensional

morphometry, a precise volumetric determination (using microcomputed tomography, for instance) would be more suitable to compare Mg degradation rates in soft tissue *versus* bone.

Dissimilarities also existed between soft tissue and bone in their responses to Mg implants. For example, whereas the proportions of CD68+ cells around gas voids were comparable in soft tissue and in bone marrow, bone voids were more highly surrounded by iNOS+ cells than soft tissue voids (Paper III). This finding indicated more severe inflammation in bone than in soft tissue and prompted questions regarding the influence of tissue environments on the cellular response. In fact, bone and soft tissue are constitutively very different. Our findings (Paper III) showed a density of cells in the bone marrow that was ~4 times higher than in the subcutaneous fascia in soft tissue. Moreover, the subcutaneous fascia is almost uninterrupted, while the cortical bone and the bone marrow form a semiclosed compartment. Considering these discrepancies between tissue types, it is easier to comprehend why the voids persisted after 4 weeks in bone but not in soft tissue. This also confirms previous data from *in vivo* studies that indicate, upon the insertion of Mg implants, a fast escape of hydrogen from soft tissues (within hours) [139] in contrast with the persistence of elevated hydrogen pressure in the bone marrow (several weeks) [141]. Therefore, it is evident that sustained pressure due to the release of gas and the accumulation of gas cavities cannot be excluded inside the semiclosed compartment that forms bone but is unlikely in soft tissue. Interestingly, reports from the 1990s documented a similar increase in intramedullary pressure in divers. [213]. In fact, long hyperbaric exposure and rapid decompression lead to the accumulation of nitrogen gas bubbles inside the bone marrow of long bones that elevate the bone marrow pressure. [213]. In animals, this increased pressure may profoundly alter bone marrow composition by increasing adipose tissue abundance or, occasionally, by inducing bone formation around medullary necrotic foci [214, 215].
The ability to repair or regenerate varies remarkably across different tissues. Reparative fibrosis around Mg implants is typical of the soft tissue response. However, bone elicits a more complex response, owing to its unique architecture and rich reservoir of immune cells (~3 times more tissue-resident macrophages are present in the bone marrow [216] than in the subcutaneous fascia [217]) and progenitors (cells that can undergo osteogenic, chondrogenic or adipogenic differentiation). Facets of tissue regeneration (osteogenesis *at* the bone–implant interface) and tissue repair (adipogenesis *beyond* the bone–implant interface) can, therefore, coexist in the bone response to Mg implants.

## 5.5. METHODOLOGICAL CONSIDERATIONS

When Mg implants degrade in tissues, their byproducts are not confined to the tissue–implant interface but are diffused to remote tissue territories. Therefore, a cardinal point in understanding how cells respond to Mg implant degradation *in vivo* is to resolve this interaction spatially and temporally.

Well-established animal models of implantation into soft tissue [168, 169, 218] and bone [219-221] were used to study the cellular responses in different, albeit related, biological compartments surrounding the implants that can be grossly divided into cells 'belonging' to the tissue–implant interface and cells located beyond this interface in the nearby tissue. In soft tissue (Paper I), for instance, this compartmentalization of the tissue–implant interface allowed us to correlatively monitor the morphological and compositional changes at the surface of the implants, the concentrations of $Mg^{2+}$, and the linked cellular behaviors in terms of gene and protein expression at the interface with the implants. Similarly, in bone (Paper II), a characterization of the cellular activity and distribution was achieved at the bone–implant interface and at remote distances in the surrounding bone marrow. Furthermore, the local cellular responses to gas voids were studied (Paper III) while assessing the potential impact of the void proximity to the implant on this activity. Based on information from previous experimental work in the same animal models [168, 169, 218-221], timepoints were carefully selected to monitor the initial-to-relatively long biological events following *in vivo* implant insertion. These include inflammation during the first week following implantation [172, 222], and tissue repair/regeneration leading to fibrotic encapsulation in soft tissue [169] and osseointegration in bone [219, 220], typically after 4 weeks with titanium implants in the models used.

Selecting an appropriate control biomaterial is not straightforward. For assessing Mg metallic biomaterials, the ideal control ought to be metallic, degradable, and with robust preclinical and clinical evidence supporting its biocompatibility. Nonetheless, a biomaterial that fulfills all these criteria remains elusive. This confines the choices to non-degradable metals, such as titanium, or degradable materials, such as polymers. Recognized as the state-of-the-art biocompatible non-degradable metallic biomaterial, titanium holds a core role in clinical practice with extensive clinical data demonstrating its efficacy in soft tissue and in bone. A span exceeding fifty years has yielded comprehensive preclinical information elucidating the host response to titanium [170, 173, 223-225]. In the present thesis, the cellular, molecular, and structural outcomes in soft tissue are largely in agreement with the findings from multiple studies of titanium using the same animal models [168, 169, 218-221].

## 5.6. LIMITATIONS

While designed to ultimately result in complete degradation in living tissues, Mg implants remain largely unresorbed in soft tissue and in bone by 4 weeks. Therefore, an evident limitation in the present work is the lack of information on healing progression beyond 4 weeks. This obscures opportunities to determine the long-term responses in soft tissue and bone. Studies of Mg implants in rats over long observation periods indicate that, depending on the alloy composition, the degradation kinetics can profoundly shift after 4 weeks [226]. Whether such changes in the degradation behavior of Mg implants can occur after 4 weeks in the present animal models remains unknown. This limitation also hampers answering

important questions regarding the fate of increased adiposity in the bone marrow in response to Mg implants or the altered composition of bone at the interface with pure Mg implants beyond 4 weeks.

The systemic effects of Mg implant degradation were not investigated in this thesis. It is undeniable that degradation products from Mg implants may enter the blood circulation and thereby reach other tissues and organs outside their implantation site. Recognizing that the byproducts may exert distant effects, titanium and Mg implants were inserted separately in different animals. Biochemical monitoring of the concentrations of Mg and the alloying components in plasma and urine are often combined with histological examinations of selected distal tissues/organs (heart, brain, spleen, kidney, liver, and lung) to exclude systemic cytotoxicity [39, 110]. These analyses are consistently undertaken when newly designed Mg metallic biomaterials are tested *in vivo*. However, the pure and alloyed Mg used in our studies has been extensively studied in a variety of *in vivo* experimental setups [227, 228], including rats [229]. It is, therefore, unlikely that systemic cytotoxicity will arise from the implantation of the Mg biomaterials tested in the present work. However, using systemic biomarkers to monitor the healing of Mg implants is a promising avenue awaiting exploration.

The degradation of Mg implants was monitored in the present work by a series of biochemical ($Mg^{2+}$ concentration in exudate, Paper I) and morphological [degradation layer thickness, Paper I and Paper II; gas (voids) in tissues, Paper I, III] analyses. Correlations were also established with the cellular response. However, other byproducts were not investigated. Key among these are reactive oxygen species and hydroxide ions, which elicit pH alteration. Alkaline pH due to Mg degradation is widely recognized in *in vitro* settings but is assumed to be buffered by living tissues [59]. However, information on pH changes at the interface with Mg implants *in vivo* remains largely unexplored [59, 229]. In fact, the soft tissue model used in this thesis (Paper I) can offer future opportunities for monitoring pH in the peri-implant exudate retrieved around Mg implants in correlation with changes in $Mg^{2+}$ concentration and cellular activities.

## 5.7. TRANSLATIONAL ASPECTS

Translating data from animal studies to clinical conditions is anything but a challenging task. Despite evident barriers (disparities related to species, age, and sex of the animals, intricacies of the experimental models) obscuring attempts to reflect the present data to humans directly, some insights from this work may be interpreted in a clinical context.
First, given the scarce information available on the early response *in vivo* to Mg implants, the amplified, transient proinflammatory response (Paper I, Paper II) demonstrated in this work is significant. This finding converges with a few clinical reports indicating transient local adverse effects in response to Mg osteosynthesis implants, particularly in the overlaying soft tissue [102-106]. Together with this clinical

information, the present data solidifies the notion that an intensified inflammation in soft tissue may be an expected early event in patients but should resolve as the healing advances.

Second, the cytotoxicity studies in this work present essential insights. Clinically approved Mg implants are proven safe for patients, often based on animal safety studies that explore potential systemic adverse effects using biochemical and histological tests to rule out cytotoxicity [39]. Equivalent data from humans remains scarce [51]. Our findings depicting the absence of cytotoxicity or adverse effects on the viability of cells sampled at the interface soft tissue–implant – even amidst heightened inflammation – are crucial and reinforce the notion of clinical safety of these implants.

Third, the antifibrotic effect in soft tissue (Paper I) might offer clues regarding the potential advantages of biodegradable metallic Mg-stent, although differences between tissues could lead to a response discrepancy. Tailoring Mg-based vascular stents to degrade slower could attenuate undesired fibrosis-related restenosis in treated vessels more effectively.

Fourth, the observed increase in bone marrow adiposity and its potential link with gas voids raises pertinent questions on the fate of the medullary adipose in patients treated with Mg osteosynthesis implants. This concern becomes even more pressing in pediatric and elderly patients, or under compromised conditions. While clinical studies comparing Mg implant degradation across different age groups are lacking, animal studies indicate rapid degradation of Mg implants in older animals [230]. These studies also suggest that a substantially quick degradation prevents Mg implants from osseointegration in osteoporotic animals in contrast with successful osseointegration in control old and juvenile animals [230]. These observations highlight the need for a closer examination of bone marrow associated with Mg implants in bone, with particular attention to gas evolution in tissues adjacent to the implants and at remote locations from them.

Fifth and lastly, given that pure Mg implants alter the composition of the new interfacial bone, whether such alteration has any implication on the functional loading in patients requires evaluation. Obvious ethical obstacles, however, challenge this. In this context, the study of samples retrieved from patients with failing implants [107] becomes crucial and offers a direct window into the specificities of the human response to Mg implants. Such patient-derived data requires a synergistic collaboration among clinicians, pathologists, and *in vivo* experimentalists to fill the gap between preclinical findings and clinical outcomes and to advance the understanding of the response to Mg implants.

# *6. Summary & Conclusions*

– In soft tissue (Paper I), the degradation of pure Mg implants amplified the initial inflammation in comparison to that seen with nondegradable titanium implants. This observation contradicts the alleged anti-inflammatory effect ascribed to Mg and Mg-based implants. At the soft tissue-Mg implant interface, a profuse initial release of degradation products, which peaked at 3 d, caused increased inflammatory cell recruitment and fostered gene and protein expression of proinflammatory and neoangiogenesis markers up to 6 d postimplantation with no cytotoxic impact. Intensified inflammation was also exhibited by sham sites remote (~2 cm) from the interface of soft tissue–Mg implants with tissue cavities resembling gas voids. The subsequent decrease in $Mg^{2+}$ concentrations and the development of protective layers rich in calcium and phosphorus at the surfaces of Mg implants permitted inflammation to markedly subside and facilitated the transition to appropriate tissue repair. Mg implants encouraged the assembly of a fibrous capsule that featured improved vascularization and reduced thickness in comparison to that at the soft tissue interface with titanium implants. Overall, the degradation dynamics of Mg implants tuned the initial inflammation and regulated the subsequent reparative processes of fibrosis and angiogenesis in soft tissue.

– In bone (Paper II), pure and alloyed Mg implants elicited the onset of a strong proinflammatory response in comparison to those of nondegradable titanium implants. An initial activation of proinflammatory macrophages and osteoclasts in conjunction with a stimulation of angiogenesis was seen at the interface with pure and alloyed Mg implants. However, this inflammatory response to both types of Mg implants was transient and was followed by reinforced reparative osteogenesis and enhanced osseointegration. Importantly, the faster degradation of pure Mg implants sustained a low-intensity inflammation that resulted in previously unknown tissue alterations at the implant interface and beyond: the newly formed bone at the surface of pure Mg was 'younger', and the bone marrow remotely located from the pure Mg implant interface enclosed an increased adiposity in comparison to that seen with alloyed Mg and titanium implants. Overall, as demonstrated in soft tissue, Mg implants in bone elicited an initial immunomodulation that promoted osseointegration; however, when Mg implant degradation quickens, a compositional alteration of the interfacial bone and an increase in bone marrow adiposity may occur.

– Gas voids (Paper III) in soft tissue and in bone induced a proinflammatory environment by strongly attracting cells and encouraging them to adopt a proinflammatory phenotype. However, the magnitude of this inflammatory response was tissue-dependent. Gas voids in bone marrow exhibited more severe inflammation and a potential connection to adipose growth. A previously unknown link to mechanosensation was also suggested by the increased expression

of Piezo type mechanosensitive ion channel component 1 (PIEZO1) in cells neighboring gas voids in both tissue types. An increased expression of PIEZO1 at the interface of Mg implants with both tissues was also shown for the first time. Occasionally, a hitherto unreported mineralized bone matrix was observed around voids in the bone marrow. Rather than mere reservoirs of gas, gas voids appear to play more intricate, multifaceted roles that combine inflammation and mechanosensation.

Having these conclusions in mind, it becomes pertinent to revisit the questions raised in the Introduction of this thesis: *Are Mg metallic biomaterials biocompatible? And are they bioactive?*
The data in the present thesis negate *in vivo* local cytotoxicity due to the degradation of Mg implants and support their ability to steer appropriate tissue repair and regeneration. These results, demonstrated through a suite of cellular, morphological, and compositional studies on the properties of Mg implants in comparison to those of the state-of-the-art biocompatible metallic biomaterial (i.e., titanium), concur, therefore, with the notion of biocompatibility of Mg metallic biomaterials. This research also demonstrated that Mg implants can efficiently promote angiogenesis and osteogenesis, underscoring the bioactivity of these biomaterials.

Above all, this thesis highlights the dynamism inherent to the host–Mg implant interaction which shapes a spatiotemporally changing tissue landscape. It is, therefore, reasonable to conceive that both the biocompatibility and bioactivity of Mg implants are, likewise, dynamic rather than static. Reflecting this dynamism is, for example, the novel finding in this work showing an intensified but transient inflammation that precedes tissue repair and regeneration. This challenges the prevalent notion attributing anti-inflammatory properties to these biomaterials. Another example is the stimulation of the osteoclastic activity that was demonstrated in this thesis to precede osteogenesis and stands against the widely accepted anti-osteoclastic effect ascribed to Mg metallic biomaterials. A final example of this dynamism that was unveiled in this work is the increased bone marrow adiposity and the altered composition of the interfacial new bone that was elicited only by the fast(er) degradation of pure Mg implants.

Finally, by demonstrating for the first time the effects of inflammation and mechanosensation by the gas voids in tissues around Mg implants, this thesis demonstrates that the notions of biocompatibility and bioactivity may be expanded outside the confines of the host–implant interface to degradation products of Mg implants, i.e., gas voids. Such a holistic understanding of the spatial and time-resolved host–Mg implant interaction is key for the interpretation of clinical observations and future tailoring of Mg implants.

# 7. Future perspectives

The findings of the present thesis accentuate the influence of immunomodulation by Mg implant degradation on the programming of healing phenotypes. At the confines of the interface with the implants and beyond, adaptative behaviors of cells and rearrangements of tissues can be equally dictated by the implant and its degradation products. The data of the present thesis validates the benefits of employing Mg implants in fulfilling their reparative task in different tissue environments. However, it also points toward the need to further comprehend the delicate interplay between inflammation, Mg degradation, and tissue repair/regeneration to better predict the clinical outcomes. It would be, therefore, relevant to explore the following question:

***Influence of age and compromised conditions on the inflammatory response and subsequent repair/regeneration:*** Mg implants degrade quicker in old than in juvenile animals [230]. Can an uncontrolled inflammation accelerate implant degradation? Moreover, how does it alter tissue repair and regeneration? Equally intriguing is the influence of different disease conditions on degradation and the respective tissue response. Why do Mg implants fail in osteoporotic [230] animals while they rescue impaired fracture healing in animals under bisphosphonates [231]? Also, what is the effect of irradiation on Mg implant healing?

***Fate and growth mechanisms of the bone marrow adiposity:*** Exploring the long-term fate of the increased bone marrow adiposity is equally important as determining the influence of other degradation products on its growth. Adipose dysfunction is suggested to be linked with oxidative stress. Then, what is the influence of reactive oxygen species released from Mg implants on bone marrow adipose?

***Link Interoception–mechanotransduction around gas voids:*** The role of neuropeptides such calcitonin gene-related polypeptide-α (CGRP) is well established in $Mg^{2+}$-associated osteogenesis [120]. Emerging evidence suggests a relationship between mechanosensation and sensory neurons [232]. So, can gas voids also elicit the release of neurotransmitters via mechanotransduction during Mg implant healing?

***Transcriptomic fingerprint of the gas voids versus tissue–implant interface:*** To further unveil the mechanisms behind the effect of gas in shaping the healing response to Mg implants, spatially resolved transcriptomics would offer undeniable benefits.

***Monitoring of gas voids in living systems:*** Imaging of gas voids is sparking debates among clinicians, with multiple questions on the challenges of radiographically interpreting Mg implants and gas voids in patients. Tools directed

at imaging tissue–Mg implant interfaces, such as magnetic resonance imaging and photoacoustic imaging, were at the core of the EU- Marie Skłodowska-Curie Actions network 'MgSafe' from which the present doctoral project stems. Refining these techniques for enhanced *in vivo* visualization of gas voids could prove important in untangling their biological significance and clinical interpretation.

# *Acknowledgement*

Moving to Sweden marked a new chapter of my life as I commenced my PhD, full of excitement about embarking on an EU-project, and at a place that I had dreamed of since my undergraduate years. I promised myself to do my best. Then, the pandemic came, and introduced unforeseen challenges. Since, the path has been demanding but exceptionally rewarding. As I look back, profound gratitude fills me for the support and kindness from many, that made navigating this journey possible.

Foremost among those to whom I owe immense gratitude is my main supervisor, Peter Thomsen. His mentorship has been invaluable to me. I found not just an academic guide but someone who consistently provided strength and support, much like a father would. His dedication to my growth and success has profoundly impacted both my academic and personal life. I am deeply grateful for his guidance and encouragement at every step of the way. It is beyond words.

Each of my co-supervisors, Anders Palmquist, Omar Omar, and Furqan Ali Shah, brought unique strengths, and their support was a driving force behind this work. I sincerely thank Anders for the pivotal insights throughout my PhD journey and for the refreshing breaks filled with French chats. Merci beaucoup! I am deeply grateful to Omar for his commitment to offering precious advice, feedback, and assistance in research, and more. I genuinely thank Furqan for supporting me with his extensive knowledge and for being a source of ideas and inspiration.

Immense thanks go to Lena Emanuelsson, Birgitta Norlindh, Anna Johansson Loo, and Maria Hoffmann for their invaluable support even during the toughest moments of the pandemic. Without their help and expertise, completing my PhD would have been impossible. I would thank them for always offering assistance in the midst of their own demanding workloads. Huge thanks to Rose Marie Tschina and Magnus Wassenius for always offering precious suggestions and solutions for administrative matters.

To every member of the 'MgSafe' network, thank you for sharing your expertise, your valuable contribution, and the fruitful scientific exchange. Working in collaboration with you was such a learning experience. Special thanks go particularly to all the co-authors from the network at the Warsaw University of Technology, Poland, and at Hereon Geesthacht, Germany. Thank you, Diana Martinez, for your help, patience, and friendship.

I cannot forget all the delightful moments with all the current and previous PhDs and postdocs at the department. Special thanks to Martina Jolić, Adam Turner, Paula Giraldo, Jincy Philip, Chiara Micheletti, Marsel Ganeyev, Reza Mokhtari, Marcel Kunrath, and Liliana Morales Laverde for their friendship, and for all the

laughs when trying to decipher what is written on our room's white table, the funny moments at the Journalé clubbé, and the nice stories at *fika*. Profound thanks to Farah, a friend who was always there to help, listen, and support me throughout my PhD journey.

I would also like to thank Margarita Trobos, Hanna Aludden, Christer Dahlin, Martin Johansson, Tomas Albrektsson, and Pentti Tengvall for the nice discussions.

I owe a debt of gratitude to Prof. Ki-Tae Koo my master's degree supervisor, at Seoul University, South Korea. The opportunity he gave me was a turning point in my academic journey. I will never forget his kindness and support!

To Elisabeth whose presence in my life blended the warmth of a mother with the bond of a true friend. Thank you for always being there.

Finally, to my mother and my father for all your sacrifices and boundless love, this work is for you. To my wife Imene, for her enduring patience and continuous backing, your love and care have meant more than words can express.

Financial support was received from the project "Promoting patient safety by a novel combination of imaging technologies for biodegradable magnesium implants, MgSafe" funded by the European Training Network within the framework of Horizon 2020 Marie Skłodowska-Curie Action (MSCA) (811226) (www.mgsafe.eu); the Swedish Research Council (2020-04715; 2018-02891); the Swedish state under the agreement between the Swedish government and the county councils, the ALF agreement (ALFGBG-725641); the IngaBritt and Arne Lundberg Foundation; the Sylvan Foundation; the Hjalmar Svensson Foundation (2020–95; 2021-271); and the Area of Advance Materials of Chalmers and GU Biomaterials within the Strategic Research Area initiative launched by the Swedish government.

# *References*


1. Zhang, X. and D. Williams, Definitions of biomaterials for the twenty-first century. 2019: Elsevier.
2. Socialstyrelsen. Statistikdatabasen. 2023; Available from: https://www.socialstyrelsen.se/statistik-och-data/statistik/statistikdatabasen/.
3. Prediger, B., et al., Elective removal vs. retaining of hardware after osteosynthesis in asymptomatic patients-a scoping review. Syst Rev, 2020. 9(1): p. 225.
4. Patel, R., Periprosthetic Joint Infection. N Engl J Med, 2023. 388(3): p. 251-262.
5. Trobos, M., et al., Genomics of Staphylococcus aureus and Staphylococcus epidermidis from Periprosthetic Joint Infections and Correlation to Clinical Outcome. Microbiol Spectr, 2022. 10(4): p. e0218121.
6. Zaborowska, M., et al., Immunomodulatory effects exerted by extracellular vesicles from Staphylococcus epidermidis and Staphylococcus aureus isolated from bone-anchored prostheses. Biomaterials, 2021. 278: p. 121158.
7. Bostman, O. and H. Pihlajamaki, Routine implant removal after fracture surgery: a potentially reducible consumer of hospital resources in trauma units. J Trauma Acute Care Surg, 1996. 41(5): p. 846-849.
8. Kellam, P.J., et al., Complications of hardware removal. J Bone Joint Surg Am, 2021. 103(22): p. 2089-2095.
9. Aspenberg, P., Silk, metal and bone: why take implants out? Nat Rev Rheumatol, 2014. 10(7): p. 386-387.
10. Loder, R.T. and J.R. Feinberg, Orthopaedic implants in children: survey results regarding routine removal by the pediatric and nonpediatric specialists. J Pediatr Orthop, 2006. 26(4): p. 510-519.
11. Writing Group for, C.-C., et al., Understanding clinical and non-clinical decisions under uncertainty: a scenario-based survey. BMC Med Inform Decis Mak, 2016. 16(1): p. 153.
12. Aspenberg, P., Why do we operate proximal humeral fractures? 2015, Taylor & Francis: Acta Orthop, 2015. p. 279-279.
13. Raney, E.M., et al., Evidence-based analysis of removal of orthopaedic implants in the pediatric population. J Pediatr Orthop, 2008. 28(7): p. 701-704.
14. Wang, X., et al., The Necessity of Implant Removal after Fixation of Thoracolumbar Burst Fractures—A Systematic Review. J Clin Med, 2023. 12(6): p. 2213.
15. Reith, G., et al., Metal implant removal: benefits and drawbacks–a patient survey. BMC Surg, 2015. 15: p. 1-8.
16. Sigwart, U., et al., Intravascular stents to prevent occlusion and re-stenosis after transluminal angioplasty. N Engl J Med, 1987. 316(12): p. 701-706.
17. Farb, A., et al., Morphological predictors of restenosis after coronary stenting in humans. Circulation, 2002. 105(25): p. 2974-2980.
18. Fattori, R. and T. Piva, Drug-eluting stents in vascular intervention. Lancet, 2003. 361(9353): p. 247-249.

19. Finn, A.V., et al., Vascular responses to drug eluting stents: importance of delayed healing. Arterioscler Thromb Vasc Biol, 2007. 27(7): p. 1500-1510.
20. Bosman, W., et al., Infections of intravascular bare metal stents: a case report and review of literature. Eur J Vasc Endovasc Surg, 2014. 47(1): p. 87-99.
21. Law, M.A. and V.S. Tivakaran, Coarctation of the aorta. 1995.
22. Magee, A., et al., Stent implantation for aortic coarctation and recoarctation. Heart, 1999. 82(5): p. 600-606.
23. González-Calle, A., I. Guillén-Rodríguez, and F. Coserria-Sánchez, Timing of surgical repair of the stented aortic arch and coarctation in neonates. Cardiol Young, 2023. 33(1): p. 147-148.
24. Schranz, D., et al., Bioabsorbable metal stents for percutaneous treatment of critical recoarctation of the aorta in a newborn. Catheter Cardiovasc Interv, 2006. 67(5): p. 671-673.
25. Boshoff, D.E., et al., Endovascular stenting of juvenile vessels: consequence of surgical stent removal on vessel architecture. Eur Heart J, 2007. 28(8): p. 1033-1036.
26. Li, C., et al., Design of biodegradable, implantable devices towards clinical translation. Nat Rev Mater, 2020. 5(1): p. 61-81.
27. Colombo, A. and E. Karvouni, Biodegradable Stents: "Fulfilling the Mission and Stepping Away". 2000, Am Heart Assoc. p. 371-373.
28. Al-Shalawi, F.D., et al., Biodegradable synthetic polymer in orthopaedic application: A review. Mater Today Proc, 2023.
29. Navarro, M., et al., Biomaterials in orthopaedics. J R Soc Interface, 2008. 5(27): p. 1137-58.
30. Jinnouchi, H., et al., Fully bioresorbable vascular scaffolds: lessons learned and future directions. Nat Rev Cardiol, 2019. 16(5): p. 286-304.
31. Han, H.-S., et al., Current status and outlook on the clinical translation of biodegradable metals. Mater Today, 2019. 23: p. 57-71.
32. Retegi-Carrión, S., et al., The effect of Ca2+ and Mg2+ ions loaded at degradable PLA membranes on the proliferation and osteoinduction of MSCs. Polymers, 2022. 14(12): p. 2422.
33. Zhang, J., et al., Magnesium modification of a calcium phosphate cement alters bone marrow stromal cell behavior via an integrin-mediated mechanism. Biomaterials, 2015. 53: p. 251-64.
34. Xiong, A., et al., The fabrication of a highly efficient hydrogel based on a functionalized double network loaded with magnesium ion and BMP2 for bone defect synergistic treatment. Mater Sci Eng C Mater Biol Appl, 2021. 128: p. 112347.
35. Shi, X., et al., Surface modification of titanium by hydrothermal treatment in Mg-containing solution and early osteoblast responses. J Mater Sci Mater Med, 2012. 23(5): p. 1281-90.
36. Sul, Y.T., et al., The bone response of oxidized bioactive and non-bioactive titanium implants. Biomaterials, 2005. 26(33): p. 6720-30.
37. Sul, Y.-T., C. Johansson, and T. Albrektsson, Which surface properties enhance bone response to implants? Comparison of oxidized magnesium, TiUnite, and Osseotite implant surfaces. Int J Prosthodont, 2006. 19(4).
38. Zheng, Y.F., X.N. Gu, and F. Witte, Biodegradable metals. Mater Sci Eng R Rep, 2014. 77: p. 1-34.

39. Liu, Y., et al., Fundamental theory of biodegradable metals—definition, criteria, and design. Adv Funct Mater, 2019. 29(18): p. 1805402.
40. Williams, D.F., Corrosion of implant materials. Annu Rev Mater Res, 1976. 6(1): p. 237-266.
41. Esmaily, M., et al., Fundamentals and advances in magnesium alloy corrosion. Prog Mater Sci, 2017. 89: p. 92-193.
42. Gray-Munro, J.E. and M. Strong, The mechanism of deposition of calcium phosphate coatings from solution onto magnesium alloy AZ31. J Biomed Mater Res A, 2009. 90(2): p. 339-50.
43. Gilbert, J.L. and G.W. Kubacki, Oxidative stress, inflammation, and the corrosion of metallic biomaterials: Corrosion causes biology and biology causes corrosion, in Oxidative stress and biomaterials. 2016, Elsevier. p. 59-88.
44. Kim, J. and H. Pan, Effects of magnesium alloy corrosion on biological response-Perspectives of metal-cell interaction. Prog Mater Sci, 2022: p. 101039.
45. Hench, L.L., Bioceramics: from concept to clinic. J Am Ceram Soc, 1991. 74(7): p. 1487-1510.
46. Liu, Y., Y. Zheng, and B. Hayes, Degradable, absorbable or resorbable—what is the best grammatical modifier for an implant that is eventually absorbed by the body. Sci. China Mater, 2017. 60(5): p. 377-391.
47. Payr, E. and A. Martina, Experimentelle und klinische Beiträge zur Lebernaht und leberresection (Magnesiumplattennaht)[Experimental and clinical contributions to the liver suture and liver resection (magnesium plate seam)]. Arch Klin Chir, 1905. 77: p. 962-998.
48. Lambotte, A., L'utilisation du magnesium comme materiel perdu dans l'osteosynthèse. Bull Mem Soc Nat Chir, 1932. 28(3): p. 1325-1334.
49. Witte, F., The history of biodegradable magnesium implants: a review. Acta Biomater. , 2010. 6(5): p. 1680-1692.
50. Song, G., Control of biodegradation of biocompatable magnesium alloys. Corrosion Sci, 2007. 49(4): p. 1696-1701.
51. Windhagen, H., et al., Biodegradable magnesium-based screw clinically equivalent to titanium screw in hallux valgus surgery: short term results of the first prospective, randomized, controlled clinical pilot study. Biomed Eng Online, 2013. 12(1): p. 1-10.
52. Holweg, P., et al., A lean bioabsorbable magnesium-zinc-calcium alloy ZX00 used for operative treatment of medial malleolus fractures: early clinical results of a prospective non-randomized first in man study. Bone Joint Res, 2020. 9(8): p. 477-483.
53. Lee, J.W., et al., Long-term clinical study and multiscale analysis of in vivo biodegradation mechanism of Mg alloy. Proc Natl Acad Sci U S A, 2016. 113(3): p. 716-21.
54. Erbel, R., et al., Temporary scaffolding of coronary arteries with bioabsorbable magnesium stents: a prospective, non-randomised multicentre trial. Lancet, 2007. 369(9576): p. 1869-1875.
55. Xin, Y., T. Hu, and P. Chu, In vitro studies of biomedical magnesium alloys in a simulated physiological environment: a review. Acta Biomater, 2011. 7(4): p. 1452-1459.
56. Kirkland, N., et al., A survey of bio-corrosion rates of magnesium alloys. Corrosion Sci, 2010. 52(2): p. 287-291.

57. Mei, D., et al., Selecting medium for corrosion testing of bioabsorbable magnesium and other metals–a critical review. Corrosion Sci, 2020. 171: p. 108722.
58. Fischer, J., et al., Reprint of: Improved cytotoxicity testing of magnesium materials. Mater Sci Eng B, 2011. 176(20): p. 1773-1777.
59. Wang, J., et al., Recommendation for modifying current cytotoxicity testing standards for biodegradable magnesium-based materials. Acta Biomater, 2015. 21: p. 237-249.
60. Sanchez, A.H.M., et al., Mg and Mg alloys: how comparable are in vitro and in vivo corrosion rates? A review. Acta Biomater, 2015. 13: p. 16-31.
61. Makkar, P., et al., In-vitro and in-vivo evaluation of strontium doped calcium phosphate coatings on biodegradable magnesium alloy for bone applications. Appl Surf Sci, 2020. 510: p. 145333.
62. Gao, J., Y. Su, and Y.-X. Qin, Calcium phosphate coatings enhance biocompatibility and degradation resistance of magnesium alloy: Correlating in vitro and in vivo studies. Bioact Mater, 2021. 6(5): p. 1223-1229.
63. Liu, J., et al., In vitro and in vivo studies of Mg-30Sc alloys with different phase structure for potential usage within bone. Acta Biomater, 2019. 98: p. 50-66.
64. Walker, J., et al., The in vitro and in vivo evaluation of the biocompatibility of Mg alloys. Biomed Mater, 2013. 9(1): p. 015006.
65. Li, W., et al., In vitro and in vivo studies on ultrafine-grained biodegradable pure Mg, Mg–Ca alloy and Mg–Sr alloy processed by high-pressure torsion. Biomater Sci, 2020. 8(18): p. 5071-5087.
66. Williams, D.F., Definitions in biomaterials:. 1987, Amsterdam: Elsevier.
67. Williams, D., General Concepts of Biocompatibility. Handbook of biomaterial properties. 1998, New York J. Black, G.W. Hastings (Eds.). 563-570.
68. Anderson, J.M., Future challenges in the in vitro and in vivo evaluation of biomaterial biocompatibility. Regen Biomater, 2016. 3(2): p. 73-77.
69. Xia, D., et al., Research status of biodegradable metals designed for oral and maxillofacial applications: A review. Bioact Mater, 2021. 6(11): p. 4186-4208.
70. Messersmith, P.B., Multitasking in tissues and materials. Science, 2008. 319(5871): p. 1767-1768.
71. Witte, F., et al., In vivo corrosion of four magnesium alloys and the associated bone response. Biomaterials, 2005. 26(17): p. 3557-63.
72. Zberg, B., P.J. Uggowitzer, and J.F. Löffler, MgZnCa glasses without clinically observable hydrogen evolution for biodegradable implants. Nat. Mater., 2009. 8(11): p. 887-891.
73. Williams, D.F., Biocompatibility pathways and mechanisms for bioactive materials: The bioactivity zone. Bioact Mater, 2022. 10: p. 306-322.
74. Hench, L.L., et al., Bonding mechanisms at the interface of ceramic prosthetic materials. J Biomed Mater Res, 1971. 5(6): p. 117-141.
75. Xu, B., et al., Magnesium metal and its corrosion products: Promising materials for tumor interventional therapy. J Magnes Alloys, 2023.
76. Saha, S., et al., Corrosion in Mg-alloy biomedical implants-the strategies to reduce the impact of the corrosion inflammatory reaction and microbial activity. J Magnes Alloys, 2022.
77. Wang, J.L., et al., Biodegradable magnesium-based implants in orthopedics—a general review and perspectives. Adv. Sci. (Weinh), 2020. 7(8): p. 1902443.

78. Kim, D.J., et al., Magnesium intake in relation to systemic inflammation, insulin resistance, and the incidence of diabetes. Diabetes Care, 2010. 33(12): p. 2604-2610.
79. Gile, J., et al., Magnesium: The overlooked electrolyte in blood cancers? Blood Rev, 2020. 44: p. 100676.
80. Kanellopoulou, C., et al., Mg2+ regulation of kinase signaling and immune function. J Exp Med, 2019. 216(8): p. 1828-1842.
81. Larsson, S.C., N. Orsini, and A. Wolk, Dietary magnesium intake and risk of stroke: a meta-analysis of prospective studies. Am J Clin Nutr, 2012. 95(2): p. 362-366.
82. Nielsen, F.H., Magnesium deficiency and increased inflammation: current perspectives. J Inflamm Res, 2018: p. 25-34.
83. Costello, R.B., et al., Perspective: the case for an evidence-based reference interval for serum magnesium: the time has come. Adv Nutr, 2016. 7(6): p. 977-993.
84. King, D.E., et al., Magnesium intake and serum C-reactive protein levels in children. Magnes Res, 2007. 20(1): p. 32-36.
85. Rodríguez-Morán, M. and F. Guerrero-Romero, Elevated concentrations of TNF-alpha are related to low serum magnesium levels in obese subjects. Magnes Res, 2004. 17(3): p. 189-196.
86. Tam Tam, H.B., et al., Magnesium sulfate ameliorates maternal and fetal inflammation in a rat model of maternal infection. Am J Obstet Gynecol, 2011. 204(4): p. 364 e1-8.
87. Chaigne-Delalande, B., et al., Mg2+ regulates cytotoxic functions of NK and CD8 T cells in chronic EBV infection through NKG2D. Science, 2013. 341(6142): p. 186-91.
88. Lötscher, J., et al., Magnesium sensing via LFA-1 regulates CD8+ T cell effector function. Cell, 2022. 185(4): p. 585-602. e29.
89. Obstetricians, A.C.o. and Gynecologists, Practice Bulletin No. 171: management of preterm labor. Obstet Gynecol, 2016. 128(4): p. e155-e164.
90. Sugimoto, J., et al., Magnesium decreases inflammatory cytokine production: a novel innate immunomodulatory mechanism. J Immunol, 2012. 188(12): p. 6338-6346.
91. De Baaij, J.H., J.G. Hoenderop, and R.J. Bindels, Magnesium in man: implications for health and disease. Physiol Rev, 2015.
92. Jin, L., et al., A biodegradable Mg-based alloy inhibited the inflammatory response of THP-1 cell-derived macrophages through the TRPM7–PI3K–AKT1 signaling axis. Front Immunol, 2019. 10: p. 2798.
93. Negrescu, A.-M., et al., In vitro macrophage immunomodulation by poly (ε-caprolactone) based-coated AZ31 Mg Alloy. Int J Mol Sci, 2021. 22(2): p. 909.
94. Costantino, M., et al., Inflammatory response to magnesium-based biodegradable implant materials. Acta Biomater, 2020. 101: p. 598-608.
95. Zhao, J., et al., The beneficial potential of magnesium-based scaffolds to promote chondrogenesis through controlled Mg2+ release in eliminating the destructive effect of activated macrophages on chondrocytes. Biomater Adv, 2022. 134: p. 112719.
96. Sun, L., et al., In vitro immunomodulation of magnesium on monocytic cell toward anti-inflammatory macrophages. Regen Biomater, 2020. 7(4): p. 391-401.

97. Sabate, M., et al., Magnesium-based resorbable scaffold versus permanent metallic sirolimus-eluting stent in patients with ST-segment elevation myocardial infarction: the MAGSTEMI randomized clinical trial. Circulation, 2019. 140(23): p. 1904-1916.
98. Ortega-Paz, L., et al., Magnesium-based resorbable scaffold vs permanent metallic sirolimus-eluting stent in patients with ST-segment elevation myocardial infarction: 3-year results of the MAGSTEMI randomised controlled trial. EuroIntervention, 2022. 18(5): p. e389.
99. Oliver, A.A., et al., Recent advances and directions in the development of bioresorbable metallic cardiovascular stents: Insights from recent human and in vivo studies. Acta Biomater, 2021. 127: p. 1-23.
100. Sukotjo, C., et al., Is There a Role for Absorbable Metals in Surgery? A Systematic Review and Meta-Analysis of Mg/Mg Alloy Based Implants. Materials (Basel), 2020. 13(18): p. 3914.
101. Leigheb, M., et al., Osteosynthesis devices in absorbable Magnesium alloy in comparison to standard ones: A systematic review on effectiveness and safety. Acta Bio Medica: Atenei Parmensis, 2021. 92(Suppl 3).
102. Plaass, C., et al., Early results using a biodegradable magnesium screw for modified chevron osteotomies. J Orthop Res, 2016. 34(12): p. 2207-2214.
103. Acar, B., et al., Comparison of bioabsorbable magnesium versus titanium screw fixation for modified distal chevron osteotomy in hallux valgus. Biomed. Res. Int., 2018. 2018.
104. May, H., et al., Bioabsorbable magnesium screw versus conventional titanium screw fixation for medial malleolar fractures. J Orthop Traumatol, 2020. 21(1): p. 1-8.
105. Kose, O., et al., Fixation of medial malleolar fractures with magnesium bioabsorbable headless compression screws: short-term clinical and radiological outcomes in eleven patients. Arch Orthop Trauma Surg, 2018. 138(8): p. 1069-1075.
106. Klauser, H., Internal fixation of three-dimensional distal metatarsal I osteotomies in the treatment of hallux valgus deformities using biodegradable magnesium screws in comparison to titanium screws. Foot Ankle Surg., 2019. 25(3): p. 398-405.
107. Wichelhaus, A., J. Emmerich, and T. Mittlmeier, A case of implant failure in partial wrist fusion applying magnesium-based headless bone screws. Case Rep Orthop, 2016: 7049130.
108. Sundfeldt, M., et al., Aseptic loosening, not only a question of wear: a review of different theories. Acta Orthop, 2006. 77(2): p. 177-97.
109. Mishra, P.K., et al., Sterile particle-induced inflammation is mediated by macrophages releasing IL-33 through a Bruton's tyrosine kinase-dependent pathway. Nat Mater, 2019. 18(3): p. 289-297.
110. Suljevic, O., et al., Immunological reaction to magnesium-based implants for orthopedic applications. What do we know so far? A systematic review on in vivo studies. Mater Today Bio, 2022. 15: p. 100315.
111. Qiao, W., et al., TRPM7 kinase-mediated immunomodulation in macrophage plays a central role in magnesium ion-induced bone regeneration. Nat Commun, 2021. 12(1): p. 2885.

112. Thomsen, P., et al., Structure of the interface between rabbit cortical bone and implants of gold, zirconium and titanium. J Mater Sci Mater Med, 1997. 8: p. 653-665.
113. Yoshizawa, S., et al., Magnesium ion stimulation of bone marrow stromal cells enhances osteogenic activity, simulating the effect of magnesium alloy degradation. Acta Biomater, 2014. 10(6): p. 2834-2842.
114. Leem, Y.H., et al., Magnesium ions facilitate integrin alpha 2-and alpha 3-mediated proliferation and enhance alkaline phosphatase expression and activity in hBMSCs. J Tissue Eng Regen Med, 2016. 10(10): p. E527-E536.
115. Hung, C.-C., et al., The role of magnesium ions in bone regeneration involves the canonical Wnt signaling pathway. Acta Biomater, 2019. 98: p. 246-255.
116. Li, R.W., et al., The influence of biodegradable magnesium alloys on the osteogenic differentiation of human mesenchymal stem cells. J Biomed Mater Res A, 2014. 102(12): p. 4346-4357.
117. Zhang, X., et al., Ion channel functional protein kinase TRPM7 regulates Mg ions to promote the osteoinduction of human osteoblast via PI3K pathway: In vitro simulation of the bone-repairing effect of Mg-based alloy implant. Acta Biomater, 2017. 63: p. 369-382.
118. Wu, L., et al., Effects of extracellular magnesium on the differentiation and function of human osteoclasts. Acta Biomater, 2014. 10(6): p. 2843-2854.
119. Zhai, Z., et al., The effect of metallic magnesium degradation products on osteoclast-induced osteolysis and attenuation of NF-kappaB and NFATc1 signaling. Biomaterials, 2014. 35(24): p. 6299-310.
120. Zhang, Y., et al., Implant-derived magnesium induces local neuronal production of CGRP to improve bone-fracture healing in rats. Nat Med, 2016. 22(10): p. 1160-1169.
121. Li, Y., et al., Biodegradable magnesium combined with distraction osteogenesis synergistically stimulates bone tissue regeneration via CGRP-FAK-VEGF signaling axis. Biomaterials, 2021. 275: p. 120984.
122. Maier, J.A., et al., High concentrations of magnesium modulate vascular endothelial cell behaviour in vitro. Biochim Biophys Acta Mol Basis Dis, 2004. 1689(1): p. 6-12.
123. Han, H.S., et al., Biodegradable Magnesium Alloys Promote Angio-Osteogenesis to Enhance Bone Repair. Adv Sci (Weinh), 2020. 7(15): p. 2000800.
124. Xu, L., R. Willumeit-Romer, and B.J.C. Luthringer-Feyerabend, Mesenchymal Stem Cell and Oxygen Modulate the Cocultured Endothelial Cells in the Presence of Magnesium Degradation Products. ACS Appl Bio Mater, 2021. 4(3): p. 2398-2407.
125. Yoshizawa, S., et al., An in vivo model to assess magnesium alloys and their biological effect on human bone marrow stromal cells. Acta Biomater, 2015. 28: p. 234-239.
126. Heublein, B., et al., Biocorrosion of magnesium alloys: a new principle in cardiovascular implant technology? Heart, 2003. 89(6): p. 651-656.
127. Shah, F.A., Osteocytes as indicators of bone quality-multiscale structure-composition characterisation of the bone-implant interface (PhD thesis). 2017.

128. Anderson, T., et al., Magnesium implants in orthopaedic surgery create a diagnostic conundrum: A radiology case series and literature review. Ir J Med Sci, 2023. 192(3): p. 1381-1385.
129. Delsmann, M.M., et al., Radiolucent zones of biodegradable magnesium-based screws in children and adolescents-a radiographic analysis. Arch Orthop Trauma Surg, 2023. 143(5): p. 2297-2305.
130. Waelti, S.L., et al., Radiographic features of magnesium-based bioabsorbable screw resorption in paediatric fractures. Pediatr Radiol, 2022. 52(12): p. 2368-2376.
131. Waelti, S.L., et al., Prospective Evaluation of Magnetic Resonance Imaging Features of Magnesium-Based Alloy Screw Resorption in Pediatric Fractures. J Clin Med, 2023. 12(8).
132. Song, G. and S. Song, A possible biodegradable magnesium implant material. Advanced Engineering Materials, 2007. 9(4): p. 298-302.
133. Ohsawa, I., et al., Hydrogen acts as a therapeutic antioxidant by selectively reducing cytotoxic oxygen radicals. Nat Med, 2007. 13(6): p. 688-694.
134. Ge, L., et al., Molecular hydrogen: a preventive and therapeutic medical gas for various diseases. Oncotarget, 2017. 8(60): p. 102653-102673.
135. Papapetropoulos, A., et al., Hydrogen sulfide is an endogenous stimulator of angiogenesis. Proc Natl Acad Sci U S A, 2009. 106(51): p. 21972-21977.
136. Payr, E., Ueber Verwendung von Magnesium zur Behandlung von Blutgefässerkrankungen. Langenbecks Arch Klin Chir Ver Dtsch Z Chir, 1902. 63: p. 503-511.
137. Wilflingseder, P., R. Martin, and C. Papp, Magnesium seeds in the treatment of lymph-and haemangiomata: Revival of an old method. Eur J Plast Surg, 1981. 6: p. 105-116.
138. Staindl, O., Treatment of hemangiomas of the face with magnesium seeds. Arch Otorhinolaryngol, 1989. 246: p. 213-217.
139. Kuhlmann, J., et al., Fast escape of hydrogen from gas cavities around corroding magnesium implants. Acta Biomater, 2013. 9(10): p. 8714-8721.
140. Kim, Y.K., et al., Gas formation and biological effects of biodegradable magnesium in a preclinical and clinical observation. Sci Technol Adv Mater, 2018. 19(1): p. 324-335.
141. Zhao, D., et al., In vivo quantification of hydrogen gas concentration in bone marrow surrounding magnesium fracture fixation hardware using an electrochemical hydrogen gas sensor. Acta Biomater, 2018. 73: p. 559-566.
142. Amerstorfer, F., et al., Long-term in vivo degradation behavior and near-implant distribution of resorbed elements for magnesium alloys WZ21 and ZX50. Acta Biomater, 2016. 42: p. 440-450.
143. Schoon, J., et al., Metal-Specific Biomaterial Accumulation in Human Peri-Implant Bone and Bone Marrow. Adv Sci (Weinh), 2020. 7(20): p. 2000412.
144. Ben Amara, H., et al., Magnesium implant degradation provides immunomodulatory and proangiogenic effects and attenuates peri-implant fibrosis in soft tissues. Bioact Mater, 2023. 26: p. 353-369.
145. Duda, G.N., et al., The decisive early phase of bone regeneration. Nat Rev Rheumatol, 2023. 19(2): p. 78-95.
146. Whitaker, R., et al., Immunomodulatory biomaterials for tissue repair. Chem Rev, 2021. 121(18): p. 11305-11335.

147. Nourshargh, S. and R. Alon, Leukocyte migration into inflamed tissues. Immunity, 2014. 41(5): p. 694-707.
148. Eming, S.A., P. Martin, and M. Tomic-Canic, Wound repair and regeneration: mechanisms, signaling, and translation. Sci Transl Med, 2014. 6(265): p. 265sr6-265sr6.
149. Wynn, T.A. and K.M. Vannella, Macrophages in tissue repair, regeneration, and fibrosis. Immunity, 2016. 44(3): p. 450-462.
150. Peiseler, M. and P. Kubes, More friend than foe: the emerging role of neutrophils in tissue repair. J Clin Invest, 2019. 129(7): p. 2629-2639.
151. Schlundt, C., et al., The multifaceted roles of macrophages in bone regeneration: a story of polarization, activation and time. Acta Biomater, 2021. 133: p. 46-57.
152. Suska, F., et al., IL-1α, IL-1β and TNF-α secretion during in vivo/ex vivo cellular interactions with titanium and copper. Biomaterials, 2003. 24(3): p. 461-468.
153. Suska, F., et al., In vivo/ex vivo cellular interactions with titanium and copper. J Mater Sci Mater Med, 2001. 12(10): p. 939-944.
154. Marasco, W., E. Becker, and J. Oliver, The ionic basis of chemotaxis. Separate cation requirements for neutrophil orientation and locomotion in a gradient of chemotactic peptide. Am J Pathol, 1980. 98(3): p. 749.
155. Choi, S., et al., Biochemical activity of magnesium ions on human osteoblast migration. Biochem Biophys Res Commun, 2020. 531(4): p. 588-594.
156. Qiao, W., et al., Sequential activation of heterogeneous macrophage phenotypes is essential for biomaterials-induced bone regeneration. Biomaterials, 2021. 276: p. 121038.
157. Niethammer, P., et al., A tissue-scale gradient of hydrogen peroxide mediates rapid wound detection in zebrafish. Nature, 2009. 459(7249): p. 996-999.
158. Kwesiga, M.P., et al., Biodegradable magnesium materials regulate ROS-RNS balance in pro-inflammatory macrophage environment. Bioact Mater, 2023. 23: p. 261-273.
159. Gill, H.S., et al., Molecular and immune toxicity of CoCr nanoparticles in MoM hip arthroplasty. Trends Mol Med, 2012. 18(3): p. 145-155.
160. Silva, E.L., et al., The reduction of dissolved oxygen during magnesium corrosion. ChemistryOpen, 2018. 7(8): p. 664-668.
161. Zeller-Plumhoff, B., et al., Oxygen-sensitive nanoparticles reveal the spatiotemporal dynamics of oxygen reduction during magnesium implant biodegradation. Npj Mater Degrad, 2022. 6(1): p. 95.
162. Egners, A., M. Erdem, and T. Cramer, The response of macrophages and neutrophils to hypoxia in the context of cancer and other inflammatory diseases. Mediators Inflamm, 2016. 2016.
163. Biswas, S.K. and A. Mantovani, Orchestration of metabolism by macrophages. Cell Metab, 2012. 15(4): p. 432-437.
164. Qiao, W., et al., TRPM7 kinase-mediated immunomodulation in macrophage plays a central role in magnesium ion-induced bone regeneration. Nat. Commun., 2021. 12(1): p. 1-15.
165. Oh, M.H., J. Jang, and J.H. Lee, Polarization of THP-1-Derived Macrophage by Magnesium and MAGT1 Inhibition in Wound Healing. Archives of Plastic Surgery, 2023. 50(04): p. 432-442.

166. Eming, S.A., T.A. Wynn, and P. Martin, Inflammation and metabolism in tissue repair and regeneration. Science, 2017. 356(6342): p. 1026-1030.
167. Wynn, T.A. and T.R. Ramalingam, Mechanisms of fibrosis: therapeutic translation for fibrotic disease. Nat Med, 2012. 18(7): p. 1028-1040.
168. Suska, F., et al., In vivo cytokine secretion and NF-κB activation around titanium and copper implants. Biomaterials, 2005. 26(5): p. 519-527.
169. Suska, F., et al., Fibrous capsule formation around titanium and copper. J. Biomed. Mater. Res. A, 2008. 85(4): p. 888-896.
170. Holgers, K.-M., et al., Titanium in soft tissues, in Titanium in medicine. 2001, Springer. p. 513-560.
171. Jansson, E., et al., Ex vivo PMA-induced respiratory burst and TNF-α secretion elicited from inflammatory cells on machined and porous blood plasma clot-coated titanium. Biomaterials, 2002. 23(13): p. 2803-2815.
172. Gretzer, C., et al., H2O2 production by cells on titanium and polystyrene surfaces using an in vivo model of exudate and surface related cell function. J Mater Sci Mater Med, 2002. 13(8): p. 735-743.
173. Palmquist, A., et al., Titanium oral implants: surface characteristics, interface biology and clinical outcome. J R Soc Interface, 2010. 7(suppl_5): p. S515-S527.
174. Linder, L. and J. Lundskog, Incorporation of stainless steel, titanium and vitallium in bone. Injury, 1975. 6(4): p. 277-285.
175. Spiller, K.L., et al., Sequential delivery of immunomodulatory cytokines to facilitate the M1-to-M2 transition of macrophages and enhance vascularization of bone scaffolds. Biomaterials, 2015. 37: p. 194-207.
176. Gurevich, D.B., et al., Live imaging of wound angiogenesis reveals macrophage orchestrated vessel sprouting and regression. EMBO J, 2018. 37(13): p. e97786.
177. O'Brien, E.M., G.E. Risser, and K.L. Spiller, Sequential drug delivery to modulate macrophage behavior and enhance implant integration. Adv. Drug. Deliv. Rev., 2019. 149: p. 85-94.
178. Lacey, D.L., et al., Osteoprotegerin ligand is a cytokine that regulates osteoclast differentiation and activation. Cell, 1998. 93(2): p. 165-76.
179. Zheng, H., et al., RANKL stimulates inducible nitric-oxide synthase expression and nitric oxide production in developing osteoclasts. An autocrine negative feedback mechanism triggered by RANKL-induced interferon-beta via NF-kappaB that restrains osteoclastogenesis and bone resorption. J Biol Chem, 2006. 281(23): p. 15809-20.
180. Huang, R., et al., RANKL-induced M1 macrophages are involved in bone formation. Bone Res, 2017. 5: p. 17019.
181. Omar, O.M., et al., The stimulation of an osteogenic response by classical monocyte activation. Biomaterials, 2011. 32(32): p. 8190-204.
182. Sweet, M.J. and D.A. Hume, Endotoxin signal transduction in macrophages. J Leukoc Biol, 1996. 60(1): p. 8-26.
183. Castellani, C., et al., Bone–implant interface strength and osseointegration: Biodegradable magnesium alloy versus standard titanium control. Acta Biomater, 2011. 7(1): p. 432-440.
184. Lee, J.-W., et al., Long-term clinical study and multiscale analysis of in vivo biodegradation mechanism of Mg alloy. Proc Natl Acad Sci U S A, 2016. 113(3): p. 716-721.

185. Zhou, H., et al., Magnesium-based biomaterials as emerging agents for bone repair and regeneration: From mechanism to application. J Magnes Alloys, 2021. 9(3): p. 779-804.
186. Wu, L., et al., Effects of extracellular magnesium extract on the proliferation and differentiation of human osteoblasts and osteoclasts in coculture. Acta Biomater, 2015. 27: p. 294-304.
187. Shan, Z., et al., Development of degradable magnesium-based metal implants and their function in promoting bone metabolism (A review). J Orthop Translat, 2022. 36: p. 184-193.
188. Li, Z., et al., Development, regulation, metabolism and function of bone marrow adipose tissues. Bone, 2018. 110: p. 134-140.
189. Weisberg, S.P., et al., Obesity is associated with macrophage accumulation in adipose tissue. J Clin Invest, 2003. 112(12): p. 1796-1808.
190. Chavakis, T., V.I. Alexaki, and A.W. Ferrante, Jr., Macrophage function in adipose tissue homeostasis and metabolic inflammation. Nat Immunol, 2023. 24(5): p. 757-766.
191. Kawai, T., M.V. Autieri, and R. Scalia, Adipose tissue inflammation and metabolic dysfunction in obesity. Am J Physiol Cell Physiol, 2021. 320(3): p. C375-C391.
192. Takeshita, S., et al., Age-related marrow adipogenesis is linked to increased expression of RANKL. J Biol Chem, 2014. 289(24): p. 16699-710.
193. Chu, W., et al., Exposure to high levels of magnesium disrupts bone mineralization in vitro and in vivo. Ann Transl Med, 2020. 8(21).
194. Zhang, J., et al., Dual function of magnesium in bone biomineralization. Adv Healthc Mater, 2019. 8(21): p. 1901030.
195. Shah, F.A., K. Ruscsak, and A. Palmquist, Transformation of bone mineral morphology: From discrete marquise-shaped motifs to a continuous interwoven mesh. Bone Rep, 2020. 13: p. 100283.
196. Niethammer, P., et al., A tissue-scale gradient of hydrogen peroxide mediates rapid wound detection in zebrafish. Nature, 2009. 459(7249): p. 996-9.
197. Weavers, H., et al., Systems Analysis of the Dynamic Inflammatory Response to Tissue Damage Reveals Spatiotemporal Properties of the Wound Attractant Gradient. Curr Biol, 2016. 26(15): p. 1975-1989.
198. Chen, M., et al., Hydrogen protects lung from hypoxia/re-oxygenation injury by reducing hydroxyl radical production and inhibiting inflammatory responses. Sci Rep, 2018. 8(1): p. 8004.
199. Du, H., et al., Tuning immunity through tissue mechanotransduction. Nat Rev Immunol, 2023. 23(3): p. 174-188.
200. Wu, J., A.H. Lewis, and J. Grandl, Touch, tension, and transduction–the function and regulation of Piezo ion channels. Trends Biochem Sci, 2017. 42(1): p. 57-71.
201. Qin, L., et al., Roles of mechanosensitive channel Piezo1/2 proteins in skeleton and other tissues. Bone Res, 2021. 9(1): p. 44.
202. Solis, A.G., et al., Mechanosensation of cyclical force by PIEZO1 is essential for innate immunity. Nature, 2019. 573(7772): p. 69-74.
203. Liu, H., et al., Piezo1 channels as force sensors in mechanical force-related chronic inflammation. Front Immunol, 2022. 13: p. 816149.

204. Baratchi, S., et al., Transcatheter aortic valve implantation represents an anti-inflammatory therapy via reduction of shear stress–induced, piezo-1–mediated monocyte activation. Circulation, 2020. 142(11): p. 1092-1105.
205. Atcha, H., et al., Mechanically activated ion channel Piezo1 modulates macrophage polarization and stiffness sensing. Nat Commun, 2021. 12(1): p. 3256.
206. Chen, S., et al., Piezo1-mediated mechanotransduction promotes entheseal pathological new bone formation in ankylosing spondylitis. Ann Rheum Dis, 2023. 82(4): p. 533-545.
207. Zhang, Q., et al., Heterotopic ossification of tendon and ligament. J Cell Mol Med, 2020. 24(10): p. 5428-5437.
208. Sun, W., et al., The mechanosensitive Piezo1 channel is required for bone formation. Elife, 2019. 8: p. e47454.
209. Chen, P., et al., Mechanosensitive Piezo1 in endothelial cells promotes angiogenesis to support bone fracture repair. Cell Calcium, 2021. 97: p. 102431.
210. Hwang, C.D., et al., Contemporary perspectives on heterotopic ossification. JCI Insight, 2022. 7(14).
211. Bowen, P.K., J. Drelich, and J. Goldman, Magnesium in the murine artery: probing the products of corrosion. Acta Biomater, 2014. 10(3): p. 1475-83.
212. Hong, D., et al., Controlling magnesium corrosion and degradation-regulating mineralization using matrix GLA protein. Acta Biomater, 2019. 98: p. 142-151.
213. Kawashima, M., et al. Pathogenesis and prevention of dysbaric osteonecrosis. in Proceedings of the 12th Meeting of the United States-Japan Cooperative Program in Natural Resources (UJNR): Panel on Diving Physiology, Washington, DC, July 13-14, 1993. 1995. US Department of Commerce, National Oceanic and Atmospheric Administration.
214. Kitano, M., et al., Experimentally Induced Dysbaric Osteonecrosis in Sheep: a Histopathological Analysis. South Pacific Study. 13(2): p. 175-182.
215. Kitano, M., et al., Histopathological Study of the Bone Marrow of Rabbit Femora with Experimentally Induced Acute Decompression Sickness: with consideration of pathogenesis of dysbaric osteonecrosis in diver's femur. South Pacific Study, 1994. 14(2): p. 223-231.
216. Chang, M.K., et al., Osteal tissue macrophages are intercalated throughout human and mouse bone lining tissues and regulate osteoblast function in vitro and in vivo. J Immunol, 2008. 181(2): p. 1232-1244.
217. Rodrigues, M. and G.C. Gurtner, Black, white, and gray: macrophages in skin repair and disease. Curr Pathobiol Rep, 2017. 5: p. 333-342.
218. Svensson, S., et al., A novel soft tissue model for biomaterial-associated infection and inflammation - bacteriological, morphological and molecular observations. Biomaterials, 2015. 41: p. 106-21.
219. Branemark, R., et al., Biomechanical characterization of osseointegration during healing: an experimental in vivo study in the rat. Biomaterials, 1997. 18(14): p. 969-78.
220. Lenneras, M., et al., Oxidized Titanium Implants Enhance Osseointegration via Mechanisms Involving RANK/RANKL/OPG Regulation. Clin Implant Dent Relat Res, 2015. 17 Suppl 2: p. e486-500.

221. Shah, F.A., et al., Direct communication between osteocytes and acid-etched titanium implants with a sub-micron topography. J Mater Sci Mater Med, 2016. 27: p. 1-9.
222. Omar, O., et al., In vivo gene expression in response to anodically oxidized versus machined titanium implants. J Biomed Mater Res A, 2010. 92(4): p. 1552-66.
223. Albrektsson, T., et al., Osseointegrated titanium implants: requirements for ensuring a long-lasting, direct bone-to-implant anchorage in man. Acta Orthop Scand, 1981. 52(2): p. 155-170.
224. Linder, L., et al., Electron microscopic analysis of the bone-titanium interface. Acta Orthop Scand, 1983. 54(1): p. 45-52.
225. Shah, F.A., P. Thomsen, and A. Palmquist, Osseointegration and current interpretations of the bone-implant interface. Acta Biomater, 2019. 84: p. 1-15.
226. Kraus, T., et al., The influence of biodegradable magnesium implants on the growth plate. Acta Biomater, 2018. 66: p. 109-117.
227. Waizy, H., et al., In vivo study of a biodegradable orthopedic screw (MgYREZr-alloy) in a rabbit model for up to 12 months. J Biomater Appl, 2014. 28(5): p. 667-75.
228. Sui, B., et al., High-purity Mg and Mg-1Ca alloys: Comparative assessment of the merits regarding degradation, osteogenesis, and biosafety for orthopedic applications. J Mater Sci Technol, 2023. 140: p. 58-66.
229. Yu, Y., H. Lu, and J. Sun, Long-term in vivo evolution of high-purity Mg screw degradation - Local and systemic effects of Mg degradation products. Acta Biomater, 2018. 71: p. 215-224.
230. Sommer, N.G., et al., Implant degradation of low-alloyed Mg–Zn–Ca in osteoporotic, old and juvenile rats. Acta Biomater, 2022. 147: p. 427-438.
231. Zheng, N., et al., Magnesium facilitates the healing of atypical femoral fractures: A single-cell transcriptomic study. Mater Today, 2022.
232. Hill, R.Z., et al., PIEZO1 transduces mechanical itch in mice. Nature, 2022. 607(7917): p. 104-110.